haematologica
Journal of the Ferrata Storti Foundation

QKI dysregulation induces extensive splicing changes in T-cell acute lymphoblastic leukemia

by Bruno Palhais, Nitesh D. Sharma, Igor Fijalkowski, Tim Pieters, Dieter Deforce, Filip Van Nieuwerburgh, Pieter Mestdagh, Panagiotis Ntziachristos, Ksenia Matlawska-Wasowska and Pieter Van Vlierberghe

Received: March 25, 2025.
Accepted: December 30, 2025.

Citation: Bruno Palhais, Nitesh D. Sharma, Igor Fijalkowski, Tim Pieters, Dieter Deforce, Filip Van Nieuwerburgh, Pieter Mestdagh, Panagiotis Ntziachristos, Ksenia Matlawska-Wasowska and Pieter Van Vlierberghe. QKI dysregulation induces extensive splicing changes in T-cell acute lymphoblastic leukemia.
Haematologica. 2026 Jan 15. doi: 10.3324/haematol.2025.287809 [Epub ahead of print]

OKI dysregulation induces extensive splicing changes in T-cell acute lymphoblastic leukemia

Bruno Palhais[1,2,3,4,^,*], **Nitesh D. Sharma**[5,6,*], **Igor Fijalkowski**[1,2,4], **Tim Pieters**[1,2,3,4,7], **Dieter Deforce**[2,8,9], **Filip Van Nieuwerburgh**[2,8,9], **Pieter Mestdagh**[1,2,10,^,#], **Panagiotis Ntziachristos**[1,2,4,^,#], **Ksenia Matlawska-Wasowska**[5,6,^,#], **Pieter Van Vlierberghe**[1,2,3,#,†]

[1] Center for Medical Genetics, Ghent University and University Hospital, Ghent, Belgium
[2] Cancer Research Institute Ghent (CRIG), Ghent, Belgium
[3] Normal and Malignant Hematopoiesis Lab, Department of Biomolecular Medicine, Ghent University, Ghent, Belgium
[4] Leukemia Therapy Resistance Unit, Department of Biomolecular Medicine, Ghent University, Ghent, Belgium
[5] Department of Cell, Developmental and Integrative Biology, University of Alabama at Birmingham, Birmingham, AL, USA
[6] Department of Pediatrics, University of New Mexico, Albuquerque, NM, USA
[7] Unit for Translational Research in Oncology, Department of Diagnostic Sciences, Ghent University, Ghent, Belgium
[8] Laboratory of Pharmaceutical Biotechnology, Department of Pharmaceutics, Ghent University, Ghent, Belgium
[9] NXTGNT, Ghent University, Ghent, Belgium
[10] OncoRNALab, Department of Biomolecular Medicine, Ghent University, Ghent, Belgium
[†]Deceased
*co-first authors
[#]co-senior authors

[^]Corresponding authors

Ksenia Matlawska-Wasowska: kmatlawska@uab.edu
Panagiotis Ntziachristos: panagiotis.ntziachristos@ugent.be
Pieter Mestdagh: pieter.mestdagh@ugent.be Bruno Palhais: bruno.palhais@ugent.be

ORCID IDs:
Bruno Palhais: 0000-0003-3733-6256
Nitesh D. Sharma: 0000-0002-6228-0488
Igor Fijalkowski: 0000-0002-3212-5516
Tim Pieters: 0000-0002-2958-0104
Dieter Deforce: 0000-0002-0635-661X
Filip Van Nieuwerburgh: 0000-0001-8815-5485
Pieter Mestdagh: 0000-0001-7821-9684
Panagiotis Ntziachristos: 0000-0001-6374-8954
Ksenia Matlawska-Wasowska: 0000-0002-9903-5793
Pieter Van Vlierberghe: 0000-0001-9063-7205
Short title: *OKI* dysregulation induces extensive splicing changes in T-ALL

Author contributions

Bruno Palhais: Conceptualization, Formal Analysis, Data curation, Visualization, Investigation, Methodology, Writing – Original Draft. Nitesh D. Sharma: Investigation,

Formal Analysis, Writing – Review & Editing. Igor Fijalkowski: Data Interpretation, Writing – Review & Editing. Tim Pieters: Data Interpretation, Writing – Review & Editing. Dieter Deforce: Resources, Methodology, Investigation. Filip Van Nieuwerburgh: Resources, Methodology, Investigation. Pieter Mestdagh: Supervision, Study Design, Data Interpretation. Panagiotis Ntziachristos: Funding Acquisition, Conceptualization, Supervision, Study Design, Data Interpretation, Project Administration, Writing – Review & Editing. Ksenia Matlawska-Wasowska: Funding Acquisition, Conceptualization, Supervision, Study Design, Data Interpretation, Writing – Review & Editing. Pieter Van Vlierberghe: Funding Acquisition, Conceptualization, Supervision, Study Design, Data Interpretation, Project Administration.

Acknowledgements

We thank Sara Dufour from the VIB Proteomics Core (PRC) for her valuable assistance with the analysis of the proteomics data.

Funding

This study is supported by the Baillet Latour Grant for Medical research 2018 granted to Pieter Van Vlierberghe and the Bilateral research cooperation China (FWO) [grant number G0E6222N]. The Matlawska lab is supported by grants from the National Cancer Institute (NCI) at the National Institutes of Health (NIH) [grant numbers R01 CA237165, R01 CA282701]. The Ntziachristos laboratory is supported by the Research Foundation Flanders (FWO) [grant numbers G0F4721N, G0A8B24N]; start-up funds from the Department of Biomolecular Medicine, Ghent University, a Flanders interuniversity consortium grant [grant number BOF.IBO.2023.0006.02]; and Cancer Research Institute Ghent (CRIG) partnership grant.

Conflict of interest statement

The authors declare no conflict of interest.

Data availability statement

All raw RNA-Seq data generated in this study have been deposited in NCBI's Gene Expression Omnibus (GEO, https://www.ncbi.nlm.nih.gov/geo/) under accession number GSE281561. The proteomics data have been deposited in the PRIDE repository (https://www.ebi.ac.uk/pride/) and are accessible under accession number PXD058761.

RNA-Seq data for T-ALL cell lines from Leo et al.[35] were retrieved from Sequence Read Archive (SRA) under accession number PRJNA707100, while RNA-Seq data from CCLE[36] were accessed via SRA under accession number PRJNA523380. To facilitate comparison between cell lines, only those with at least two replicates were included in the analysis.

The RNA-seq data for primary T-ALL samples analyzed in this study are publicly available through the Database of Genotypes and Phenotypes (dbGaP) under the parent accession number phs000218 and its substudy accession number phs000464 (TARGET: Acute Lymphoblastic Leukemia (ALL) Expansion Phase 2)[3] and the Sequence Read Archive (SRA) under accession number PRJNA434176 (Verboom cohort)[32]. Additionally, RNA-seq data for 24 healthy thymocyte samples reported by Sun et al. (2021) were retrieved from the SRA under accession number PRJNA741323. All datasets, encompassing both primary T-ALL samples and healthy thymocytes, were integrated and normalized using the DESeq2 package in R.

The methylation data from T-ALL cell lines was obtained from GEO under accession number GSE68379 (Infinium HumanMethylation 450 BeadChip) and PRJNA523380 (CCLE).

Abstract

Understanding the molecular mechanisms underlying T-cell acute lymphoblastic leukemia (T-ALL) is essential for developing more effective therapeutic strategies. Despite therapeutic advances, the role of RNA-binding proteins in the pathogenesis of T-ALL remains poorly understood. Here, we investigate the RNA-binding protein Quaking (QKI), identifying it as a key regulator of splicing with tumor-suppressive properties in T-ALL. Through the analysis of two independent pediatric T-ALL cohorts, we demonstrate that *QKI* expression is frequently reduced in T-ALL, particularly within the HOXA subtype, and this reduction correlates with poor overall and event-free survival. Using T-ALL cell lines, we show that QKI depletion induces widespread splicing alterations, with numerous events corroborated in patient samples. Transcriptome profiling indicates that *QKI* downregulation leads to broad changes in gene expression, notably affecting pathways related to cell cycle progression, cholesterol homeostasis, and epithelial–mesenchymal transition. Functional assays demonstrate that *QKI* overexpression in T-ALL cells significantly reduces cell proliferation, induces G0/G1 cell cycle arrest, and limits leukemia progression and dissemination, ultimately improving survival in xenograft models. Together, these findings provide compelling evidence that *QKI* functions as a regulator of RNA splicing with tumor-suppressive activity in T-ALL.

Introduction

T-cell acute lymphoblastic leukemia (T-ALL) is an aggressive hematologic malignancy originating from the malignant transformation of T-cell precursors. Accounting for approximately 15% of pediatric and 25% of adult acute lymphoblastic leukemia (ALL) cases, T-ALL is characterized by a high degree of genetic and molecular heterogeneity [1,2]. T-ALL patients can be classified into different molecular subgroups based on transcriptome profiles and genomic alterations of specific oncogenic transcription factors, such as TAL1, TLX1, TLX3, HOXA9/10, LMO2 or NKX2-1[3,4]. Although intensified chemotherapy regimens have significantly improved survival rates, relapse remains a major challenge and is often associated with a poor prognosis. Furthermore, aggressive chemotherapy regimens are accompanied by severe short- and long-term side effects[5,6]. Therefore, understanding the molecular mechanisms underlying T-ALL is crucial for developing more effective treatments and improving patient outcomes and their quality of life.

While advances in molecular biology have provided valuable insights into the genetic basis of T-ALL, the intricate regulatory mechanisms governing its pathogenesis remain incompletely understood. Unlike other leukemias, T-ALL and B-cell lymphoblastic leukemia (B-ALL) exhibit few or no mutations affecting splicing factors (SFs)[3,7]. However, previous studies have revealed widespread changes in their splicing landscapes, even in the absence of SF mutations. These changes are attributed to post-transcriptional or post-translational dysregulation of SFs[8–10].
Recently, attention has turned towards the role of RNA-binding proteins (RBPs) in orchestrating post-transcriptional processes that drive oncogenic transformation. Among the diverse array of RBPs, the Quaking (QKI) protein, a member of the Signal Transduction and Activation of RNA (STAR) family of RBPs, plays a pivotal role in various cellular processes through its regulation of RNA metabolism[11]. Previous studies have identified decreased *QKI* expression, along with increased expression of *HOXA* genes, as among the most significantly differentially expressed genes in T-ALL patients with MLL-rearrangements, *SET-NUP214* and *CALM-AF10* translocations compared to other T-ALL subgroups[12–15]. Additionally, we have linked reduced *QKI* expression to circular RNA dysregulation in T-ALL, underscoring its multifaceted role in leukemia biology[16].

QKI is encoded by the *QKI* gene and is involved in the regulation of mRNA splicing, stability, translation, and localization[11]. The functional diversity of *QKI* is largely attributed to the presence of multiple isoforms, which arise from alternative splicing of its pre-mRNA[17]. These isoforms include QKI-5, QKI-6, and QKI-7, each of which differs in its C-terminal region, exhibiting distinct subcellular localizations and

functions[11]. QKI-5 is predominantly nuclear and is implicated in the regulation of alternative splicing[18,19], a process in which non-coding regions called introns are excised from pre-mRNA molecules, and the remaining coding regions, known as exons, are joined together. QKI-5 interacts with specific RNA sequences, known as Quaking response elements (QREs) to influence the splicing of pre-mRNAs involved in various cellular pathways[20]. This isoform is particularly critical during developmental processes, such as myelination in the central nervous system, where it regulates the splicing of mRNAs essential for oligodendrocyte maturation and function[21]. Additionally, QKI-5 has been shown to play a role in epithelial-mesenchymal transition (EMT), a process crucial for cancer metastasis, by modulating the splicing of mRNAs that contribute to the mesenchymal phenotype[22–24]. Dysregulation of *QKI* expression has been implicated in various pathological conditions, including neurodevelopmental disorders, cardiovascular diseases, and cancer[22,25–27].

Here, we investigated the expression of *QKI* in two large, independent pediatric T-ALL cohorts. Our analysis demonstrated that *QKI* expression was decreased in T-ALL patients compared to their healthy counterparts (thymocytes). Additionally, silencing *QKI* in T-ALL cell lines allowed us to identify the pool of QKI-regulated splicing events, which were subsequently confirmed to be dysregulated in T-ALL patients with lower *QKI* expression levels. Furthermore, *QKI* expression in primary samples was highly correlated with the degree of missplicing. Through *in vivo* studies, we demonstrated that *QKI* overexpression prolongs survival and significantly reduces leukemic infiltration in multiple organs, highlighting its tumor-suppressive potential in the T-ALL models tested. In conclusion, we characterized *QKI* as an RNA-binding protein with tumor suppressive properties in T-ALL and define the dysregulated splicing landscape associated with its loss, laying the groundwork for the discovery of new therapeutic targets and prognostic markers.

Methods

For further information, see Supplemental Methods.

Cell lines

T-ALL cell lines were cultured in RPMI 1640 medium supplemented with 20% (HPB-ALL and KARPAS-45) or 10% (Jurkat, DND-41, TALL-1, LOUCY, ALL-SIL, KOPT-K1, PF-382) fetal calf serum (FCS), 100 U/mL penicillin, 100 mg/mL streptomycin, and 2 mM l-glutamine at 37°C with 5% CO_2. HEK293 cells were cultured in DMEM supplemented with 10% fetal calf serum, 100 U/mL penicillin, 100 mg/mL streptomycin, and 2 mM l-glutamine at 37°C with 5% CO_2.

Primary samples

De-identified primary patient samples were obtained from the Children's Oncology Group study ALL0434 and the University of New Mexico (IRB #16-246 and #03-183). All patients or their parents or guardians provided written, informed consent in accordance with the Declaration of Helsinki and local institutional guidelines.

Mouse in vivo experiments

NOD.Cg-Prkdcscid Il2rgtm1Wjl/SzJ (NSG) mice (6–8 weeks old) were purchased from the Jackson Laboratory and maintained in a pathogen-free, AAALAC-accredited facility. The animal experiments were approved by the Ethical Committees on animal welfare at the University of Alabama at Birmingham (IACUC-22544, IACUC-22519). The T-ALL cell lines, PF-382 and KARPAS-45, were transduced with either a control construct or a QKI expression construct. A total of 10^6 transduced T-ALL cells were injected into the tail vein of each mouse. For survival analyses, mice (n=10 per group) were euthanized upon showing signs of moribund disease and/or a weight loss of 15%. For leukemia burden analyses, animals (n=5 per group) received 10^6 transduced PF-382 or KARPAS-45 cells via tail vein injection. All mice were sacrificed at the same time point, 23 days for PF-382 and 32 days for KARPAS-45 post-engraftment. Leukemic cells were isolated from the bone marrow of femurs, blood, meninges, spleen, liver, and lungs. Cells were stained using anti-human APC-CD45 and anti-mouse BV-421-CD45 antibodies (BD Biosciences) and analyzed by flow cytometry. Data were processed using FlowJo software.

RNA Sequencing

RNA integrity was assessed and sequenced using Illumina Truseq stranded total RNA library prep (150 bp paired-end). Sequenced reads were trimmed for adapter sequences and low-quality bases using TRIMMOMATIC v0.39. Trimmed sequence reads were aligned to the human genome using STAR v2.7.11b and quantified at the transcriptome level using Salmon v1.10.3 using GRCh38 Gencode release 44 reference. Differential gene expression analysis was performed using DESeq2. GSEA was performed using Hallmark[28] gene set collections. Splicing analysis was carried out using MAJIQ v2.5.7[29]. The heterogen module was applied to primary samples, while splicing changes in cell lines were analyzed using MAJIQ deltapsi. For each local splicing variant (LSV), MAJIQ calculates the mean percent spliced in (PSI,ψ) to determine the delta PSI (Δψ) between two groups. LSVs with a Δψ greater than 0.15 (15%) and a probability of change greater than 0.95 were considered changing and subjected to further analysis. Changing LSVs were then aggregated into modules using VOILA modulize to facilitate biological interpretation of alternative splicing events.

Results

QKI is downregulated in T-ALL

Given that dysregulated splicing is common in T-ALL[9,30] and the critical role of *QKI* in splicing[18,19], we explored *QKI* gene expression in primary T-ALL samples. We analyzed publicly available RNA-Seq data from two independent pediatric patient cohorts, TARGET (n=265)[3] and Verboom et al. (n=60)[31], alongside healthy thymocytes from different developmental stages[32]. These cohorts provide comprehensive transcriptional profiles of primary T-ALL samples, enabling robust comparisons with healthy thymocytes at various developmental stages. Overall, T-ALL blasts exhibited lower *QKI* mRNA expression compared to healthy thymocytes (Figure 1A). We, next investigated whether low *QKI* expression is associated with any of the T-ALL molecular subgroups. Interestingly, T-ALL patient samples within the HOXA subgroup showed significantly lower *QKI* mRNA expression than the other subgroups (Figure 1B). In addition, analysis of a recently published T-ALL dataset with a more refined molecular subtype classification[33] revealed that *QKI* expression is significantly reduced in the NUP98, LMO2 δγ–like, MLLT10, KMT2A, and NUP214 subtypes (Supplementary Figure 1A). T-ALL can arise from the blockade of normal T-cell development, which prompted us to investigate *QKI* expression during this process. We observed that *QKI* expression remains relatively stable across all stages of normal T-cell development. (Supplementary Figure 1B). In contrast, the significantly reduced *QKI* expression observed in T-ALL deviates from this steady expression pattern, suggesting that low *QKI* levels are an abnormal feature of T-ALL rather than a reflection of normal developmental variation. Using a Cox proportional-hazards model, we assessed the relationship between *QKI* expression and overall survival of T-ALL patients in the TARGET cohort. Patients with lower *QKI* mRNA expression had worse overall survival ($p = 0.018$) and event free survival ($p = 0.053$) compared to those with high *QKI* expression (Figure 1C, Supplementary Figure 1C). To assess which *QKI* isoforms are expressed in normal T-cells, we inspected the 3'end of *QKI* transcripts using both, long-read sequencing (ONT) and short-read sequencing (Illumina) RNA-Seq data. We predominantly identified reads that were consistent with the *QKI*-5 transcript (Supplementary Figure 1D). To further identify the presence of QKI protein isoforms, we performed Western blotting with QKI-specific antibodies (anti-QKI-5, anti-QKI-6, anti-QKI-7, and anti-QKI-7B) as well as an antibody that targets all QKI isoforms (anti-Pan-QKI). Our results showed that only the QKI-5 protein was detected (Supplementary Figure 1E). To establish that T-ALL patients exhibit decreased QKI protein levels, we tested a set of primary patient samples. Our findings revealed that, among the nine patient samples examined, five had low QKI protein levels, all of which belonged to the HOXA subtype (Figure 1D). Two additional HOXA cases exhibited higher QKI expression. Decreased *QKI*

expression in T-ALL samples prompted us to examine *QKI* mutations and copy number variations (CNVs) in the TARGET cohort. We identified 8 patients with *QKI* CNVs, of which 5 were copy number loses and 3 were copy number gains (Supplementary Figure 1F). Moreover, there were no *QKI* mutations reported in this dataset. Thus, *QKI* dysregulation cannot be attributed solely to genetic mutations, suggesting that other factors are involved.

Next, we explored *QKI* expression in T-ALL cell lines by analyzing RNA-Seq data from a panel of 13 T-ALL cell lines, which included both publicly available datasets[34,35] and in-house sequenced cell lines. Upon examining *QKI* mRNA levels, we found that LOUCY and KARPAS-45 expressed the lowest levels of *QKI*, while HPB-ALL and TALL-1 exhibited high *QKI* expression (Figure 1E). Our results are consistent with a previous study in which reduced *QKI* expression in the LOUCY cell line was associated with the *SET-NUP214* fusion and elevated *HOXA* gene expression[12]. KARPAS-45 is an MLL-rearranged cell line and is also associated with high *HOXA* expression.

Transcript expression does not always result in equivalent protein abundance. Therefore, we assessed QKI protein levels using Western blotting and mass spectrometry, generating matched RNA-Seq and proteomics data for 6 T-ALL cell lines (LOUCY, KARPAS-45, DND-45, HPB-ALL, ALL-SIL, TALL-1). Linear regression analysis revealed a strong correlation between *QKI* mRNA and protein abundance ($R^2 = 0.8552$, $p < 0.001$) (Figure 1F). Immunoblotting using a QKI-5 specific antibody confirmed that QKI-5 is nearly absent in the T-ALL cell lines LOUCY and KARPAS-45 (Figure 1G). The high correlation observed between mRNA and protein suggests that *QKI* expression is mainly regulated at the transcriptional level. Given that T-ALL cases exhibit reduced *QKI* expression compared to their natural counterpart and that *QKI* genetic abnormalities are mostly absent in primary T-ALL samples, we hypothesized that epigenetic mechanisms might be responsible for the low *QKI* levels observed in T-ALL patients. It was shown that epigenetic alterations in T-ALL play a crucial role in regulating gene expression and cellular processes, leading to the silencing of tumor suppressor genes or the activation of oncogenes, which promote cell proliferation and survival[36]. Interestingly, hierarchical clustering of gene expression data from the TARGET cohort revealed that *QKI* and *TET2* display similar expression patterns (Supplementary Figure 1F). Given that *TET2* expression is silenced in T-ALL through promoter hypermethylation[37,38], we investigated whether a similar mechanism underlies the regulation of *QKI* by examining the methylation status of the *QKI* promoter in T-ALL cell lines. Genome-wide DNA methylation data from T-ALL cell lines[39] revealed that the *QKI* promoter is hypermethylated in both KARPAS-45 and LOUCY cell lines compared to other T-ALL cell lines (Figure 1H, Supplementary Figure 1G), suggesting a potential epigenetic mechanism for *QKI* dysregulation.

Taken together, our results demonstrate a significant reduction in *QKI* expression in T-ALL blasts compared to healthy thymocytes, particularly in the HOXA subgroup. This reduction in *QKI* expression is associated with a worse outcome in T-ALL patients. Data from T-ALL cell lines further support a strong correlation between QKI mRNA and protein levels.

QKI depletion leads to altered mRNA splicing in T-ALL cell lines

To characterize the impact of low *QKI* expression levels in the T-ALL splicing landscape, we silenced the main T-ALL-expressed *QKI* isoform, QKI-5, in JURKAT and HPB-ALL cells, which exhibit medium to high *QKI* expression.

We established two models for transient and stable depletion of *QKI* expression by siRNA-mediated knockdown in Jurkat cells and shRNA-mediated knockdown in HPB-ALL cells. Assessment of the knockdown efficiency by Western blotting showed a robust decrease in QKI protein abundance in both tested cell lines (Figure 2A). Subsequently, total RNA was extracted and processed for RNA-sequencing to identify changes in mRNA splicing upon *QKI* depletion. We then used MAJIQ v2[29] to perform differential splicing analysis on the RNA-Seq data obtained from each cell line. For each local splicing variant (LSV) a mean percent spliced in (PSI,ψ) value was calculated and groups were compared using the delta PSI (Δψ) metric. LSVs with a Δψ greater than 0.15 (15%; 5% FDR) were considered differentially spliced and further analyzed. A total of 252 differentially spliced LSVs were identified in Jurkat cells when comparing siQKI with siNTC, while 177 were altered when comparing shQKI with shNTC in HPB-ALL cells. These LSVs involved 185 and 137 genes in Jurkat and HPB-ALL, respectively. The analysis of the splicing changes in Jurkat and HPB-ALL cells revealed that although some events were unique to each cell line, 50 LSVs (28 genes) were common to both cell lines (Figure 2B).

To aid in interpreting the biological implications of the splicing changes, LSVs were aggregated into alternative splicing modules (the combination of possible splicing events), and the most relevant differentially spliced event was extracted. Among all the event types detected, alternative last exon events were the most commonly impacted by QKI depletion in Jurkat cells (22.5%), followed by alternative first exon (22.9%) and cassette exon (22.5%) events, whereas in HPB-ALL cells, cassette exon events were the most impacted (63.0%), followed by alternative last exon events (13.0%) (Figure 2C).

Splicing factors, such as QKI, have been shown to either promote or inhibit splice site recognition, depending on their binding sequence context[29]. Therefore, to understand the directional changes in splicing events affected by QKI depletion, we extracted and analyzed the ψ values (inclusion level) for each sample across alternatively spliced events. As expected, Jurkat and HPB-ALL samples clustered

according to the presence or absence of QKI. More importantly, two distinct splicing patterns were observed within each cell line upon QKI depletion, one cluster of splicing events with increased inclusion, and another with increased skipping (Figure 2D). Among the 52 differentially spliced modules, 23 (44%) showed increased inclusion following QKI depletion in Jurkat cells, whereas 29 (56%) showed increased skipping. Similarly, 12 out of 32 (37%) differentially spliced modules were included upon *QKI* knockdown, whereas 20 (63%) were skipped in HPB-ALL. To validate the detected splicing events, we performed independent RT-PCR on a subset of representative events using primers flanking the alternatively spliced cassette exons, confirming the splicing patterns identified in the computational analysis (Figure 2E). To further corroborate these findings, we performed siRNA mediated depletion of *QKI* in an additional T-ALL cell line with high *QKI* levels, ALL-SIL, and validated the changes observed upon QKI loss in Jurkat and HPB-ALL cells (Supplementary Figure 2).

We identified previously known QKI targets in solid tumors, including *ADD3*[26], *CD47*, *DEPDC1*[23] and *ESYT2*[22,24], *AKAP9*[27] as well as novel QKI-regulated splicing events specific to T-ALL, such as *ERBIN*, *DVL1* and *TCF12*. For instance, *QKI* knockdown led to exon inclusion in transcripts of the cell surface "don't eat me" signal *CD47*, extended synaptotagmin 2 (*ESYT2*), the Wnt/β-catenin signaling pathway component *DVL1* and the T-cell transcription factor *TCF12* (also known as *HEB*) (Figure 3A), suggesting that QKI represses the inclusion of these exons. Conversely, QKI-depleted cells exhibited exon skipping in the Wnt/β -catenin signaling pathway component *LRRFIP2*, indicating that QKI positively regulates the inclusion of this exon in the mature transcript (Figure 3B).

Taken together, the data presented here show that *QKI* modulates specific splicing events in T-ALL, which may contribute to its biological functions.

Downregulation of QKI induces global transcriptional alterations in T-ALL

Next, we sought to characterize the transcriptional landscape upon *QKI* silencing in T-ALL cells. We performed differential gene expression (DGE) analysis between shQKI and shNTC transduced HPB-ALL cells. A total of 23 genes were found to be significantly upregulated, while 101 genes were downregulated (absolute fold change > 1.5, p-value < 0.05) (Figure 4A).

To unravel the biological implications of the differentially expressed genes, we ranked them by $\log_2$ fold change and performed gene set enrichment analysis (GSEA) using the hallmark gene sets from MSigDB[28,40]. The results showed a strong positive enrichment for the gene sets of E2F targets and G2M checkpoint. Conversely, there was a negative enrichment for the cholesterol homeostasis, the epithelial to mesenchymal transition and coagulation gene sets (Figure 4B). The visualization of

the GSEA plots revealed a clear profile with the upregulated genes driving the positive enrichment score associated with the E2F targets and G2M checkpoints gene sets. Conversely, downregulated genes contributed to the negative enrichment score of the cholesterol homeostasis (Figure 4C) and coagulation gene sets (Supplementary Figure 3A). Moreover, we investigated the GSEA enrichment of the EMT gene set, a process that has been shown to be influenced by *QKI* expression[23,24]. As expected, we observed an association between downregulated genes and the EMT signature (Supplementary Figure 3A).

To gain further insights into the genes contributing to the positive enrichment of E2F targets, we explored the gene expression of the leading genes identified through GSEA analysis. A hierarchical clustering heatmap revealed a clear difference in gene expression between shNTC and shQKI HPB-ALL cells. Among the top upregulated genes were *SPC24*, *RRM2*, *CIT*, and *EZH2*, which all contribute to this transcriptional signature (Figure 4D). Consistent with the cholesterol homeostasis signature, core pathway genes were among the most downregulated in shQKI HPB-ALL cells, including *HMGCR*, *SQLE*, *SREBF2*, *LDLR* and *FDFT1*, indicating suppression of cholesterol biosynthesis and uptake (Figure 4E).

To decouple the effects of differential alternative splicing from differential gene expression, we examined the expression levels of genes that were alternatively spliced upon *QKI* depletion in HPB-ALL cells. Notably, most alternatively spliced genes showed no significant changes in overall expression (Supplementary Figure 3B). Therefore, the observed differential expression of transcripts following *QKI* depletion is likely an indirect effect, potentially mediated by some of the alternatively spliced genes rather than through direct transcriptional regulation by *QKI*.

Collectively, our findings showed that *QKI* silencing in T-ALL cells induce substantial changes in gene expression. These changes highlight *QKI*'s role in regulating key pathways related to cell proliferation and differentiation. Notably, alternative splicing and gene expression changes appear largely independent, suggesting that *QKI*'s influence on transcription may be indirect, potentially mediated through its regulation of splicing events.

QKI dysregulation induces ubiquitous aberrant splicing in T-ALL

To confirm the splicing changes driven by *QKI* in a broader range of T-ALL cell lines we compared the splicing patterns associated with endogenous *QKI* levels in a panel of T-ALL cell lines with those detected by experimental *QKI* silencing in HPB-ALL and Jurkat cells. The heatmap revealed that the splicing profiles of KARPAS-45 and LOUCY cells, which express low levels of *QKI*, displayed splicing patterns similar to those of Jurkat and HPB-ALL cells in which *QKI* was silenced, whereas cell lines with higher QKI expression exhibited distinct profiles. This further suggests that the splicing events detected by *QKI* silencing are a common feature related to

endogenous *QKI* expression, since they were also detected in other T-ALL cell lines under normal conditions (Figure 5A).

Although cell lines are useful to study and model the molecular mechanisms of diseases, they may not always accurately reflect the characteristics of T-ALL patients. To overcome this, we performed differential splicing analysis using primary samples from two independent T-ALL cohort datasets, TARGET and Verboom. First, we stratified the patients according to their *QKI* expression level. Specifically, using the kernel density estimation of *QKI* expression for all T-ALL patients, we defined patients with normalized counts lower than 800 as the QKI-low group and the remaining as QKI-high (Figure 5B). Differential splicing analysis identified additional splicing events exclusively in the primary samples that were not observed in the T-ALL cell lines, underscoring the importance of analyzing both primary samples and cell lines. Noteworthy, of the 34 splicing changes detected in T-ALL cell lines, we validated 22 in the Verboom cohort (Figure 5C) and 23 in the TARGET T-ALL cohort (Figure 5D).

Next, we examined the splicing patterns of *LRRFIP2* and *TCF12* in T-ALL patients with low and high *QKI* expression, comparing them to those typically observed in healthy thymocytes. These two genes were selected as examples because their splicing was consistently altered in both T-ALL cell lines and primary T-ALL samples based on *QKI* expression levels. In both cohorts of T-ALL patients, the levels of *LRRFIP2* exon inclusion were comparable between those with high *QKI* expression and thymocytes. In contrast, patients with low *QKI* expression exhibited *LRRFIP2* exon skipping (Supplementary Figure 4A). Low-QKI T-ALL patients exhibited significantly higher inclusion of the *TCF12* ankyrin exon compared to high-QKI patients. Notably, this exon is rarely included in *TCF12* transcripts from healthy thymocytes, suggesting its inclusion in T-ALL is an aberrant splicing event resulting from reduced *QKI* expression (Supplementary Figure 4B).

Considering that T-ALL patients exhibit a wide range of *QKI* expression, we sought to determine whether there is an association between *QKI* expression and the corresponding ψ values of the perturbed splicing events. Linear regression analysis showed a strong positive correlation between *QKI* expression and ψ values (inclusion level) for events that are activated by *QKI* (Figure 6A) and a strong negative correlation for events that are repressed (Figure 6B).

Together, the data from T-ALL cell lines and primary patient samples indicate that *QKI* dysregulation is associated with widespread splicing alterations in T-ALL, and the extent of these splicing changes closely correlate with *QKI* expression levels.

QKI negatively regulates T-ALL cell proliferation

Reduced *QKI* expression in primary samples suggests a putative tumor-suppressive role of *QKI* in T-ALL. To investigate this hypothesis, we assessed the impact of

ectopic *QKI* overexpression *in vitro* using the T-ALL cell line PF-382 and KARPAS-45. T-ALL cells were transduced with either a control construct or a *QKI* expression construct. qPCR analysis confirmed robust *QKI* overexpression in cells transduced with the QKI construct, showing approximately 20-fold and 25-fold increase in *QKI* mRNA levels in PF-382 and KARPAS-45 cells, respectively, compared with the control vector (Figure 7A, top). A concomitant increase in QKI-5 protein levels was verified by Western blot analysis (Figure 7A, bottom). A proliferation assay demonstrated that PF-382 and KARPAS-45 cells expressing higher levels of *QKI* exhibited reduced proliferation compared to control cells (Figure 7B). To further validate the growth-suppressive finction of *QKI*, we performed QKI knockdown in KOPT-K1 T-ALL cells using two independent shRNAs targeting QKI (Figure 7C). Silencing QKI resulted in a significant increase in T-ALL cell proliferation compared to control cells, suggesting that QKI negatively regulates leukemic cell growth (Figure 7D). Consistent with these findings, QKI-depleted HPB-ALL cells (shQKI) also resulted in increased cell growth compared with non-targeting control cells (shNTC) (Figure 7E). To elucidate the mechanism behind this growth difference, we examined both apoptosis and cell cycle progression. While no significant difference in apoptosis levels was detected upon either QKI overexpression or QKI silencing (Supplementary Figure 5A, 5C and 5E), we observed an arrest at G0/G1 transition in QKI-expressing T-ALL cells (Figure 7F, Supplementary Figure 5B and Supplementary Figure 5D). Conversely, *QKI* silencing in KOPT-K1 cells led to a decrease in the G0/G1 population and a corresponding increase in the G2/M fraction (Figure 7G, Supplementary Figure 5F), consistent with enhanced cell cycle progression.

Collectively, these findings demonstrate that *QKI* restrains T-ALL cell proliferation by modulating cell cycle dynamics, supporting its role as a negative regulator of leukemic cell proliferation.

QKI inhibits leukemia progression

Next, we evaluated whether *QKI* overexpression affects T-ALL engraftment and disease progression *in vivo*, using human-to-mouse xenograft models. PF-382 and KARPAS-45 cells harboring either the control or *QKI* overexpression construct were transplanted into immunocompromised mice, and survival was monitored over time. Mice transplanted with QKI-overexpressing cells had a significantly prolonged median survival than control animals (PF-382; 42 days in QKI-OE compared to 22 days in control mice; KARPAS-45; 63 days in QKI-OE compared to 35 days in control mice ($p < 0.0001$; Figure 8A and 8B), highlighting the impact of *QKI* on disease progression. Further analysis of leukemia burden, quantified by both the number and percentage of human $CD45^+$ cells, revealed that mice with QKI-overexpressing cells had significantly reduced infiltration of leukemic cells in the bone marrow, meninges,

blood, testes, liver, spleen, and lungs (Figure 8C and 8D, Supplementary Figure 6A and 6B).

Collectively, these results indicate that *QKI* functions as a negative regulator of T-ALL progression, slowing disease progression and limiting leukemia burden across multiple organs.

Discussion

This study identifies the tumor-suppressive properties of *QKI* in leukemia, contributing to disease pathogenesis through its regulation of mRNA splicing. *QKI* dysregulation appears to be a distinctive feature of T-ALL, as evidenced by its markedly lower expression levels, particularly within the HOXA subgroup, across two independent pediatric T-ALL cohorts, compared to healthy thymocytes. This is in line with previous studies showing an inverse relationship between *QKI* expression and elevated *HOXA* gene levels in cases with *KMTA2* rearrangements, *CALM-AF10*, and *SET-NUP214* translocations[12,13,15], suggesting that *QKI* may play a subtype-specific role in T-ALL. Moreover, the stable expression of *QKI* across all stages of normal T-cell development further underscores that its reduced expression in T-ALL is likely an acquired feature related to malignancy rather than a reflection of typical developmental variation. Recent findings showed that reduced *QKI* expression leads to circRNA dysregulation in T-ALL[16]. Together, these studies emphasize the significance of QKI dysregulation in driving RNA-level changes critical for T-ALL pathogenesis. The low *QKI* expression in T-ALL is significantly associated with poorer overall survival, supporting *QKI*'s potential as a prognostic marker and offering a therapeutic window to restore alternative splicing patterns disrupted by reduced *QKI* levels.

Notably, mutations or copy number losses affecting *QKI* are infrequent, observed in only a minority of patients in the TARGET cohort, pointing instead to epigenetic mechanisms as the primary drivers of *QKI* dysregulation. Consistent with this, we observed *QKI* promoter hypermethylation in the LOUCY and KARPAS-45 T-ALL cell lines, both of which exhibit minimal *QKI* expression. We and others have shown that this epigenetic regulation shapes leukemic transcriptional programs[41]. This DNA methylation-driven silencing pattern mirrors that of other tumor suppressors, such as *TET2*[37], which clustered with *QKI* in gene expression analyses (Supplementary Figure 1F) and is similarly subject to hypermethylation in T-ALL. The preferential reduction of *QKI* in HOXA-positive T-ALL, together with promoter hypermethylation in the HOXA-driven LOUCY cell line, suggests that HOXA-associated epigenetic programs may contribute to *QKI* silencing. Although we cannot definitively conclude that *HOXA* directly silences *QKI*, our data suggest that *QKI* downregulation in T-ALL is mediated by epigenetic modifications rather than

direct genetic alterations, adding *QKI* to the growing list of epigenetically regulated tumor suppressors in T-ALL.

Functional studies in cell lines and mouse models provided additional evidence that *QKI* contributes to T-ALL progression by promoting aberrant splicing and altering gene expression profiles. Furthermore, knockdown experiments in T-ALL cell lines, combined with transcriptome analyses, showed that *QKI* depletion induces significant splicing changes, especially in cassette exons, affecting genes involved in key cellular pathways such as Wnt/β-catenin signaling and EMT. Notably, we observed increased exon skipping in *LRRFIP2*, *CIT*, and *AKAP9*, along with enhanced exon inclusion in *CD47*, *ESYT2*, and *TCF12*, indicating that, as in solid tumors[23,24], *QKI* plays both repressive and activating roles in modulating splicing patterns in T-ALL. This is in line with previous reports that *QKI* displays position-dependent regulation, promoting inclusion when bound to a downstream intronic splicing enhancer (ISE) and repressing exon inclusion when bound to an upstream exonic splicing silencer (ESS)[26,29]. Importantly, these splicing changes were validated in both T-ALL cell lines and two independent T-ALL patient cohorts, highlighting the consistency of these findings across multiple models. *LRRFIP2* and *TCF12* emerged as key examples, exhibiting exon inclusion or skipping in a manner that strongly correlated with QKI expression levels in primary samples. While some of the QKI-regulated splicing changes were identified previously in solid tumors, such as *ADD3* and *CD47*, others, like *TCF12* and *ERBIN*, appear unique to T-ALL. This distinct splicing profile supports the notion that *QKI*'s role in T-ALL is influenced by the specific cellular context, potentially due to interactions with other splicing regulators that vary across tissues.

TCF12 (*HEB*) is essential for normal T-cell development[42,43] and can produce two main isoforms, a longer canonical isoform (HEBCan) and a shorter alternative isoform (HEBAlt), due to two distinct transcription start sites[44]. While HEBCan is expressed across all stages of T-cell development, HEBAlt is confined to the double-negative stages ($CD4^-CD8^-$). *QKI* depletion led to the inclusion of a 72 bp exon encoding an ankyrin-like repeat. Although this ankyrin-like exon can be incorporated into HEBCan, it was previously excluded in studies as it does not appear in transcripts from thymocyte cDNA libraries[45], suggesting it may be specifically associated with T-ALL rather than normal T-cell development. While the functional consequences of this insertion have not been extensively explored, prior research in the rat homolog (REB) showed that this insertion significantly diminished REB's ability to bind specific E-box-binding sites and to form both homodimers and heterodimers with other bHLH family members[46].

Reduced *QKI* expression in T-ALL leads to *LRRFIP2* exon 7 skipping. In gastric cancer, the isoform switching of *LRRFIP2* is regulated by the epithelial splicing regulatory protein (*ESRP1*), an epithelial-specific RNA-binding protein involved in the

alternative splicing of EMT-related genes, which are critical for metastasis. The mesenchymal isoform of *LRRFIP2* includes exon 7, promoting metastatic potential, whereas exon 7 skipping has been linked to metastasis suppression[47]. Thus, *ESRP1* acts as a negative regulator of *LRRFIP2* exon 7, while *QKI* functions as a positive splicing factor. *ESRP1* was also found to regulate the alternative splicing of *CD47*, an event which is similarly modulated by *QKI* in T-ALL. Interestingly, *ESRP1* is negligibly expressed in T-ALL (data not shown), suggesting that while *ESRP1* and *QKI* may share common splicing targets, they likely play tissue-specific roles.

The enrichment of EMT-associated pathways among the QKI-regulated splicing events and the gene expression profiles observed following *QKI* knockdown provides further insight into T-ALL biology. EMT-like changes are increasingly recognized in hematologic malignancies, where they are thought to promote cellular plasticity, invasiveness, and treatment resistance[48]. Our findings indicate that *QKI* dysregulation may induce EMT-like properties in T-ALL, potentially facilitating leukemic cell dissemination and infiltration. This aligns with reports in solid tumors where *QKI* has been shown to regulate EMT-related splicing[23,24], highlighting the conserved nature of its function across cancer types and further implicating EMT as an important mechanism in T-ALL progression.

At the transcriptomic level, *QKI* silencing led to the differential expression of hundreds of genes, impacting pathways related to cell cycle, mitosis, and the G2M checkpoint. Notably, marginal overlap between genes affected by differential expression and those with splicing alterations suggests that *QKI*'s impact on gene expression may be an indirect effect, mediated through its splicing function rather than direct transcriptional regulation. This separation of splicing and transcriptional functions reinforces the role of *QKI* as a crucial modulator of post-transcriptional regulation in T-ALL.

Our functional studies support the tumor-suppressive properties of *QKI* in T-ALL. Forced expression of *QKI* in T-ALL cell lines led to a marked reduction in cell proliferation, accompanied by G0/G1 cell cycle arrest, without significantly affecting apoptosis. Consistent with this observation, previous studies have shown that QKI-5 overexpression inhibits cell proliferation and induces G0/G1 arrest in non-small cell lung cancer (NSCLC) and clear cell renal cell carcinoma (ccRCC) cell lines[49,50]. These results underscore the conserved role of *QKI* in regulating the cell cycle across different cancer types. Collectively, these findings suggest that *QKI* inhibits leukemic growth by regulating the cell cycle rather than promoting cell death. Furthermore, *in vivo* xenograft experiments provided compelling evidence of *QKI*'s tumor-suppressive role in T-ALL, with *QKI* overexpression significantly reducing leukemia burden and extending survival in mice.

Integrating all obtained data enabled us to define the specific substrate pool of QKI-driven splicing events. Given the pervasive role of *QKI* in T-ALL, therapeutic

strategies aimed at compensating for its function loss or mitigating its downstream effects could benefit patients, particularly those within the HOXA subgroup. Potential approaches might include reversing the epigenetic silencing to partially restore QKI activity or, alternatively, targeting downstream pathways and specific splicing events that become dysregulated in the absence of sufficient QKI levels. Given the absence of *QKI* CLIP-seq or eRIC datasets and the technical difficulties of generating high-quality CLIP data for *QKI*, our study cannot directly showcase direct QKI causality to the splicing changes observed. Alternative approaches (e.g. eCLIP, TRIBE-seq) may help define direct QKI targets. Future studies are required to investigate the upstream factors and epigenetic regulators responsible for *QKI* downregulation in T-ALL, along with a deeper characterization of the isoforms and molecular mechanisms impacted by the resulting alternative splicing events.

References

1. Iacobucci I, Mullighan CG. Genetic Basis of Acute Lymphoblastic Leukemia. J Clin Oncol. 2017;35(9):975-983.

2. Hunger SP, Mullighan CG. Acute Lymphoblastic Leukemia in Children. N Engl J Med. 2015;373(16):1541-1552.

3. Liu Y, Easton J, Shao Y, et al. The genomic landscape of pediatric and young adult T-lineage acute lymphoblastic leukemia. Nat Genet. 2017;49(8):1211-1218.

4. Brady SW, Roberts KG, Gu Z, et al. The genomic landscape of pediatric acute lymphoblastic leukemia. Nat Genet. 2022;54(9):1376-1389.

5. Marks DI, Rowntree C. Management of adults with T-cell lymphoblastic leukemia. Blood. 2017;129(9):1134-1142.

6. Teachey DT, O'Connor D. How I treat newly diagnosed T-cell acute lymphoblastic leukemia and T-cell lymphoblastic lymphoma in children. Blood. 2020;135(3):159-166.

7. Chen S, Benbarche S, Abdel-Wahab O. Splicing factor mutations in hematologic malignancies. Blood. 2021;138(8):599-612.

8. Black KL, Naqvi AS, Asnani M, et al. Aberrant splicing in B-cell acute lymphoblastic leukemia. Nucleic Acids Res. 2018;46(21):11357.

9. Zhou Y, Han C, Wang E, et al. Posttranslational Regulation of the Exon Skipping Machinery Controls Aberrant Splicing in Leukemia. Cancer Discov. 2020;10(9):1388-1409.

10. Han C, Khodadadi-Jamayran A, Lorch AH, et al. SF3B1 homeostasis is critical for survival and therapeutic response in T cell leukemia. Sci Adv. 2022;8(3):eabj8357.

11. Neumann DP, Goodall GJ, Gregory PA, Philip Gregory CA. The Quaking RNA-binding proteins as regulators of cell differentiation. Wiley Interdiscip Rev RNA. 2022;13(6):e1724.

12. Van Vlierberghe P, van Grotel M, Tchinda J, et al. The recurrent SET-NUP214 fusion as a new HOXA activation mechanism in pediatric T-cell acute lymphoblastic leukemia. Blood. 2008;111(9):4668-4680.

13. Dik WA, Brahim W, Braun C, et al. CALM-AF10+ T-ALL expression profiles are characterized by overexpression of HOXA and BMI1 oncogenes. Leukemia. 2005;19(11):1948-1957.

14. Ferrando AA, Armstrong SA, Neuberg DS, et al. Gene expression signatures in MLL-rearranged T-lineage and B-precursor acute leukemias: dominance of HOX dysregulation. Blood. 2003;102(1):262-268.

15. Kang H, Sharma ND, Nickl CK, et al. Dysregulated transcriptional networks in KMT2A- and MLLT10-rearranged T-ALL. Biomark Res. 2018;6(1):27.

16. Buratin A, Palhais B, Gaffo E, et al. Depletion of the RNA binding protein QKI and circular RNA dysregulation in T-cell acute lymphoblastic leukemia. Haematologica. 2025;110(4):972-979.

17. Ebersole TA, Chen Q, Justice MJ, Artzt K. The quaking gene product necessary in embryogenesis and myelination combines features of RNA binding and signal transduction proteins. Nat Genet. 1996;12(3):260-265.

18. Wu J, Zhou L, Tonissen K, Tee R, Artzt K. The Quaking I-5 Protein (QKI-5) Has a Novel Nuclear Localization Signal and Shuttles between the Nucleus and the Cytoplasm*. J Biol Chem. 1999;274(41):29202-29210.

19. Wu JI, Reed RB, Grabowski PJ, Artzt K. Function of quaking in myelination: Regulation of alternative splicing. Proc Natl Acad Sci. 2002;99(7):4233-4238.

20. Galarneau A, Richard S. Target RNA motif and target mRNAs of the Quaking STAR protein. Nat Struct Mol Biol. 2005;12(8):691-698.

21. Bockbrader K, Feng Y. Essential function, sophisticated regulation and pathological impact of the selective RNA-binding protein QKI in CNS myelin development. Future Neurol. 2008;3(6):655-668.

22. Zong FY, Fu X, Wei WJ, et al. The RNA-Binding Protein QKI Suppresses Cancer-Associated Aberrant Splicing. Cheung VG, ed. PLoS Genet. 2014;10(4):e1004289.

23. Pillman KA, Phillips CA, Roslan S, et al. miR-200/375 control epithelial plasticity-associated alternative splicing by repressing the RNA-binding protein Quaking. EMBO J. 2018;37(13):e99016.

24. Li J, Choi PS, Chaffer CL, et al. An alternative splicing switch in FLNB promotes the mesenchymal cell state in human breast cancer. Elife. 2018;7:e37184.

25. Chen X, Yin J, Cao D, et al. The Emerging Roles of the RNA Binding Protein QKI in Cardiovascular Development and Function. Front Cell Dev Biol. 2021;9:668659.

26. Wang JZ, Fu X, Fang Z, et al. QKI-5 regulates the alternative splicing of cytoskeletal gene ADD3 in lung cancer. J Mol Cell Biol. 2021;13(5):347-360.

27. Montañés-Agudo P, Aufiero S, Schepers EN, et al. The RNA-binding protein QKI governs a muscle-specific alternative splicing program that shapes the contractile function of cardiomyocytes. Cardiovasc Res. 2023;119(5):1161-1174.

28. Liberzon A, Birger C, Thorvaldsdóttir H, Ghandi M, Mesirov JP, Tamayo P. The Molecular Signatures Database (MSigDB) hallmark gene set collection. Cell Syst. 2015;1(6):417-425.

29. Vaquero-Garcia J, Aicher JK, Jewell S, et al. RNA splicing analysis using heterogeneous and large RNA-seq datasets. Nat Commun. 2023;14(1):1230.

30. Kesel JD, Fijalkowski I, Taylor J, Ntziachristos P. Splicing dysregulation in human hematologic malignancies: beyond splicing mutations. Trends Immunol. 2022;43(8):674-686.

31. Verboom K, Van Loocke W, Volders PJ, et al. A comprehensive inventory of TLX1 controlled long non-coding RNAs in T-cell acute lymphoblastic leukemia through polyA+ and total RNA sequencing. Haematologica. 2018;103(12):e585-e589.

32. Sun V, Sharpley M, Kaczor-Urbanowicz KE, et al. The Metabolic Landscape of Thymic T Cell Development In Vivo and In Vitro. Front Immunol. 2021;12:716661.

33. Pölönen P, Di Giacomo D, Seffernick AE, et al. The genomic basis of childhood T-lineage acute lymphoblastic leukaemia. Nature. 2024;632(8027):1082-1091.

34. Leo IR, Aswad L, Stahl M, et al. Integrative multi-omics and drug response profiling of childhood acute lymphoblastic leukemia cell lines. Nat Commun. 2022;13(1):1691.

35. Ghandi M, Huang FW, Jané-Valbuena J, et al. Next-generation characterization of the Cancer Cell Line Encyclopedia. Nature. 2019;569(7757):503-508.

36. Roels J, Thénoz M, Szarzy□ska B, et al. Aging of Preleukemic Thymocytes Drives CpG Island Hypermethylation in T-cell Acute Lymphoblastic Leukemia. Blood Cancer Discov. 2020;1(3):274-289.

37. Bensberg M, Rundquist O, Selimovic A, et al. TET2 as a tumor suppressor and therapeutic target in T-cell acute lymphoblastic leukemia. Proc Natl Acad Sci U S A. 2021;118(34):e2110758118.

38. De Coninck S, Roels J, Lintermans B, et al. Tet2 is a tumor suppressor in the preleukemic phase of T-cell acute lymphoblastic leukemia. Blood Adv. 2024;8(11):2646-2649.

39. Iorio F, Knijnenburg TA, Vis DJ, et al. A Landscape of Pharmacogenomic Interactions in Cancer. Cell. 2016;166(3):740-754.

40. Subramanian A, Tamayo P, Mootha VK, et al. Gene set enrichment analysis: A knowledge-based approach for interpreting genome-wide expression profiles. Proc Natl Acad Sci. 2005;102(43):15545-15550.

41. Fang C, Wang Z, Han C, et al. Cancer-specific CTCF binding facilitates oncogenic transcriptional dysregulation. Genome Biol. 2020;21(1):247.

42. Yoganathan K, Yan A, Rocha J, et al. Regulation of the Signal-Dependent E Protein HEBAlt Through a YYY Motif Is Required for Progression Through T Cell Development. Front Immunol. 2022;13:848577.

43. Braunstein M, Anderson MK. Developmental progression of fetal HEB−/− precursors to the pre-T-cell stage is restored by HEBAlt. Eur J Immunol. 2010;40(11):3173-3182.

44. Kee BL. E and ID proteins branch out. Nat Rev Immunol. 2009;9(3):175-184.

45. Wang D, Claus CL, Vaccarelli G, et al. The Basic Helix-Loop-Helix Transcription Factor HEBAlt Is Expressed in Pro-T Cells and Enhances the Generation of T Cell Precursors. J Immunol. 2006;177(1):109-119.

46. Klein ES, Simmons DM, Swanson LW, Rosenfeld MG. Tissue-specific RNA splicing generates an ankyrin-like domain that affects the dimerization and DNA-binding properties of a bHLH protein. Genes Dev. 1993;7(1):55-71.

47. Lee J, Pang K, Kim J, et al. ESRP1-regulated isoform switching of LRRFIP2 determines metastasis of gastric cancer. Nat Commun. 2022;13(1):6274.

48. Varisli L, Vlahopoulos S. Epithelial–Mesenchymal Transition in Acute Leukemias. Int J Mol Sci. 2024;25(4):2173.

49. Zhu W, Yu Y, Fang K, et al. miR-31/QKI-5 axis facilitates cell cycle progression of non-small-cell lung cancer cells by interacting and regulating p21 and CDK4/6 expressions. Cancer Med. 2023;12(4):4590-4604.

50. Zhang RL, Yang JP, Peng LX, et al. RNA-binding protein QKI-5 inhibits the proliferation of clear cell renal cell carcinoma via post-transcriptional stabilization of RASA1 mRNA. Cell Cycle. 2016;15(22):3094-3104.

Figure legends

Figure 1. T-ALL patients exhibit low QKI expression. (**A**) Box plots of QKI mRNA expression showing that T-ALL patients from two independent cohorts (Verboom and TARGET) exhibit low QKI expression when compared to healthy thymocytes (**: $p < 0.01$; ***: $p < 0.001$; unpaired Mann-Whitney U test). (**B**) Box plots of QKI expression grouped by T-ALL molecular subtypes (****: $p < 0.0001$; Kruskal-Wallis with Dunn's post-hoc test). (**C**) Survival plot of patients from the TARGET cohort representing overall survival probabilities according to QKI expression using a Cox proportional-hazards model. The dashed line represents the baseline (average QKI expression). Patients with low QKI expression present a worse prognosis when compared to patients with high QKI high levels. (**D**) QKI protein levels in primary T-ALL patients determined by Western blotting. HOXA group samples are annotated in red. (**E**) mRNA expression of QKI in a panel of T-ALL cell lines. (**F**) Linear regression plot showing the correlation between QKI mRNA and protein levels in 6 T-ALL cell lines. (**G**) Western blot showing QKI-5 protein expression in a panel of 13 T-ALL cell lines. (**H**) QKI promoter methylation status determined by Illumina 450K BeadChip array[40].

Figure 2. QKI depletion leads to altered mRNA splicing in T-ALL cell lines. (**A**) Western blot analysis confirming QKI knockdown in Jurkat and HPB-ALL cells using siRNA (siQKI) and shRNA (shQKI), respectively. α-Tubulin was used as a loading control. (**B**) Venn diagrams showing the overlap of local splicing variants (LSVs) and genes affected by QKI knockdown in Jurkat and HPB-ALL cells. (**C**) Distribution of splicing event types upon QKI knockdown in Jurkat and HPB-ALL cells. (**D**) Heatmap of splicing changes (Z-score of ψ) in select genes across Jurkat and HPB-ALL cells upon QKI depletion, demonstrating both inclusion and skipping of exons in various transcripts. Genes in darker shade represent splicing changes detected in both Jurkat and HPB-ALL. (**E**) RT-PCR validation of QKI-dependent splicing events in Jurkat cells for CD47, ESYT2, and TCF12 transcripts, showing exon inclusion/skipping upon QKI knockdown. The higher band represents the inclusion of the cassette exon whereas the smaller band represents the exclusion.

Figure 3. QKI-dependent exon usage in *LRRFIP2* and *TCF12*. Sashimi plots depicting QKI-dependent splicing changes in LRRFIP2 (**F**) and TCF12 (**G**). The plots illustrate exon skipping/inclusion events in both Jurkat and HPB-ALL cells, as visualized through RNA-seq data.

Figure 4. QKI silencing induces widespread transcriptional changes in T-ALL cells. (**A**) Volcano plot illustrating differentially expressed genes in HPB-ALL cells transduced with shQKI compared to shNTC. A total of 23 genes were significantly upregulated, while 101 were downregulated (absolute fold change > 1.5, p-value < 0.05). (**B**) Gene Set Enrichment Analysis (GSEA) showing positive enrichment for the gene sets of E2F targets, G2M checkpoint, and negative enrichment for cholesterol homeostasis, epithelial-to-mesenchymal transition (EMT) and coagulation. (**C**) GSEA plots depicting the enrichment scores for E2F targets, G2M checkpoint, and cholesterol homeostasis. (**D**, **E**) Heatmaps displaying the top differentially expressed genes contributing to the GSEA signature for the E2F targets (top 30; ***D***) and cholesterol homeostasis (top 25; ***E***) gene sets, showing significant upregulation and downregulation, respectively, upon QKI silencing.

Figure 5. Splicing changes detected in T-ALL cell lines are corroborated in primary T-ALL samples. (**A**) Heatmap of splicing patterns in T-ALL cell lines with low QKI expression*, KARPAS*-45 and LOUCY alongside Jurkat and HPB-ALL cells where QKI was experimentally silenced and cells lines with high QKI expression. Cell lines with higher QKI expression formed a separate cluster, highlighting a common splicing signature driven by QKI levels. (B) Kernel density estimation (KDE) plot showing the distribution of QKI mRNA expression in T-ALL patient samples (both cohorts). The horizontal dashed line represents the cutoff (800) for the stratification of QKI-high and QKI-low, depending on whether patients have QKI expression above or under the cutoff, respectively. (**C**, **D**) Heatmaps representing the PSI (Ψ) values of QKI-regulated splicing events for each patient in the Verboom (**C**) and TARGET (**D**) cohorts, confirming that many splicing changes observed in cell lines are also consistently altered in both patient cohorts, according to QKI expression levels. Genes in darker shade represent concordant splicing changes detected in both primary cohorts and in T-ALL cell lines.

Figure 6. Correlation between QKI expression and alternative splicing across T-ALL patient cohorts. Linear regression plots depicting the correlation between QKI expression and the PSI (ψ) values for selected splicing events across patients from each T-ALL cohort. (**A**) Positive correlations events. (**B**) Negative correlations are events. The Spearman correlation coefficient and corresponding p-value between PSI (ψ) and QKI counts from the TARGET cohort are provided for each gene.

Figure 7. QKI regulates proliferation and cell-cycle progression in T-ALL cells. (**A**) Quantitative PCR (top) showing a significant increase in QKI mRNA levels in PF-382 and KARPAS-45 cells transduced with a QKI expression construct (QKI-OE) compared to the control construct, and Western blot (bottom) confirming elevated QKI-5 protein levels. β-actin served as the loading control. (**B**) Cell proliferation curves showing reduced growth of PF-382 and KARPAS-45 cells overexpressing QKI compared to controls over a time course of 120 hours. Data are presented as the percentage of cell growth relative to the control (****: $p < 0.0001$; repeated measure ANOVA with Tukey's multiple comparisons test). (**C**) Quantitative PCR (top) showing efficient depletion of QKI mRNA in KOPT-K1 cells transduced with two independent shRNAs targeting QKI (shQKI #1 and shQKI #2) compared to a non-targeting shRNA (shNTC), and corresponding Western blot (bottom) confirming the reduced QKI-5 protein levels. β–actin served as the loading control. (**D**) Cell proliferation curves showing increased growth of QKI-depleted KOPT-K1 cells compared with controls over 120 hours. Data are presented as the percentage of cell growth relative to the control (****: $p < 0.0001$; repeated measure ANOVA with Tukey's multiple comparisons test). (**E**) Luminescence-based proliferation assay showing significant increased cell growth in QKI-depleted HPB-ALL cells compared to shNTC after 96h (****: $p < 0.0001$; unpaired Student's t-test). (**F**) Cell cycle analysis by flow cytometry showing a significant increase in the percentage of cells arrested in the G0/G1 phase in QKI-overexpressing PF-382 and KARPAS-45 cells, compared to control cells (****: $p < 0.0001$; unpaired Student's t-test). (**G**) Cell cycle analysis by flow cytometry showing a significant reduction of QKI-depleted KOPT-K1 cells in the G0/G1 phase compared with control cells (***: $p < 0.001$; ****: $p < 0.0001$; repeated measure one-way ANOVA with Tukey's multiple comparisons test).

Figure 8. QKI overexpression prolongs survival in T-ALL xenografts. Kaplan-Meier survival curve of NSG mice transplanted via tail vein with (A) PF-382 and (B) KARPAS-45 cells transduced to overexpress QKI (yellow) or control vector (blue) (10^6 cell/mouse). demonstrating that QKI overexpression prolongs animal survival (****: $p < 0.0001$; log-rank Mantel–Cox test). (F) Leukemia burden was assessed at Day 23 for PF-382 and Day 32 for KARPAS-45 post-engraftment, determined by the infiltration of human $CD45^+$ cells in bone marrow (BM), meninges (Men.), blood, testis, liver, spleen and lungs on NSG mice inoculated with (C) PF-382 and (D) KARPAS-45 transduced T-ALL cells (10^6 cell/mouse via tail vein) (**: $p < 0.01$; ***: $p < 0.001$; ****: $p < 0.0001$; unpaired Student's t-test with Holm-Sidak multiple comparison correction).

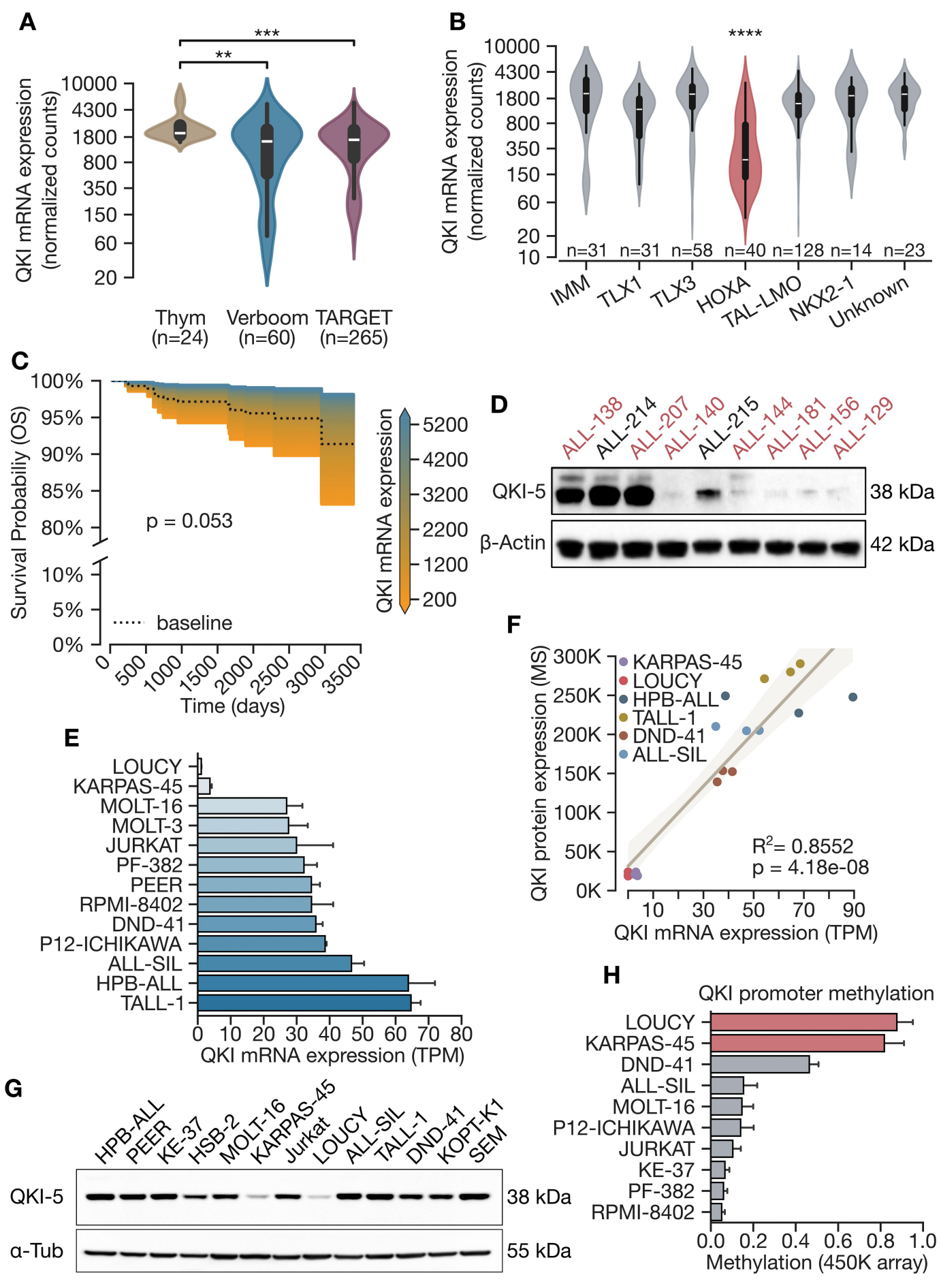
A
***
**
QKI mRNA expression (normalized counts)
10000
4300
1800
800
350
150
60
20
Thym (n=24)
Verboom (n=60)
TARGET (n=265)
B
****
QKI mRNA expression (normalized counts)
10000
4300
1800
800
350
150
60
20
10
n=31
n=31
n=58
n=40
n=128
n=14
n=23
IMM
TLX1
TLX3
HOXA
TAL-LMO
NKX2-1
Unknown
C
Survival Probabiliy (OS)
100%
95%
90%
85%
80%
10%
5%
0%
p = 0.053
baseline
0
500
1000
1500
2000
2500
3000
3500
Time (days)
QKI mRNA expression
5200
4200
3200
2200
1200
200
D
ALL-138
ALL-214
ALL-207
ALL-140
ALL-215
ALL-144
ALL-181
ALL-156
ALL-129
QKI-5
38 kDa
β-Actin
42 kDa
E
LOUCY
KARPAS-45
MOLT-16
MOLT-3
JURKAT
PF-382
PEER
RPMI-8402
DND-41
P12-ICHIKAWA
ALL-SIL
HPB-ALL
TALL-1
0
10
20
30
40
50
60
70
80
QKI mRNA expression (TPM)
F
QKI protein expression (MS)
300K
250K
200K
150K
100K
50K
0K
KARPAS-45
LOUCY
HPB-ALL
TALL-1
DND-41
ALL-SIL
R2= 0.8552
p = 4.18e-08
10
30
50
70
90
QKI mRNA expression (TPM)
G
HPB-ALL
PEER
KE-37
HSB-2
MOLT-16
KARPAS-45
Jurkat
LOUCY
ALL-SIL
TALL-1
DND-41
KOPT-K1
SEM
QKI-5
38 kDa
α-Tub
55 kDa
H
QKI promoter methylation
LOUCY
KARPAS-45
DND-41
ALL-SIL
MOLT-16
P12-ICHIKAWA
JURKAT
KE-37
PF-382
RPMI-8402
0.0
0.2
0.4
0.6
0.8
1.0
Methylation (450K array)

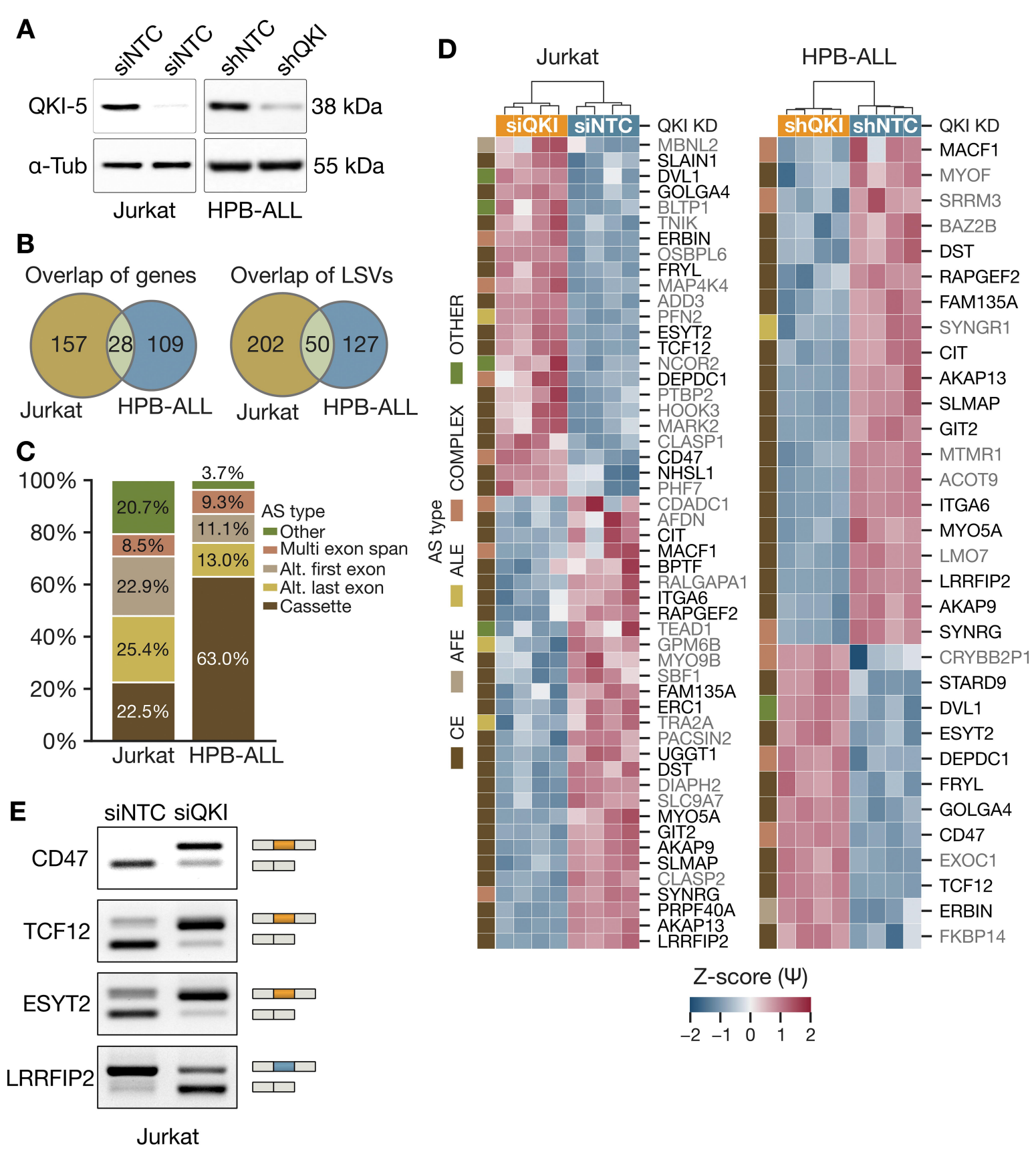
A
siNTC
siNTC
shNTC
shQKI
QKI-5
38 kDa
α-Tub
55 kDa
Jurkat
HPB-ALL
B
Overlap of genes
157
28
109
Jurkat
HPB-ALL
Overlap of LSVs
202
50
127
Jurkat
HPB-ALL
C
100%
80%
60%
40%
20%
0%
20.7%
8.5%
22.9%
25.4%
22.5%
3.7%
9.3%
11.1%
13.0%
63.0%
AS type
Other
Multi exon span
Alt. first exon
Alt. last exon
Cassette
Jurkat
HPB-ALL
D
Jurkat
HPB-ALL
siQKI
siNTC
shQKI
shNTC
QKI KD
AS type
OTHER
COMPLEX
ALE
AFE
CE
MBNL2
SLAIN1
DVL1
GOLGA4
BLTP1
TNIK
ERBIN
OSBPL6
FRYL
MAP4K4
ADD3
PFN2
ESYT2
TCF12
NCOR2
DEPDC1
PTBP2
HOOK3
MARK2
CLASP1
CD47
NHSL1
PHF7
CDADC1
AFDN
CIT
MACF1
BPTF
RALGAPA1
ITGA6
RAPGEF2
TEAD1
GPM6B
MYO9B
SBF1
FAM135A
ERC1
TRA2A
PACSIN2
UGGT1
DST
DIAPH2
SLC9A7
MYO5A
GIT2
AKAP9
SLMAP
CLASP2
SYNRG
PRPF40A
AKAP13
LRRFIP2
MACF1
MYOF
SRRM3
BAZ2B
DST
RAPGEF2
FAM135A
SYNGR1
CIT
AKAP13
SLMAP
GIT2
MTMR1
ACOT9
ITGA6
MYO5A
LMO7
LRRFIP2
AKAP9
SYNRG
CRYBB2P1
STARD9
DVL1
ESYT2
DEPDC1
FRYL
GOLGA4
CD47
EXOC1
TCF12
ERBIN
FKBP14
Z-score (Ψ)
−2
−1
0
1
2
E
siNTC
siQKI
CD47
TCF12
ESYT2
LRRFIP2
Jurkat

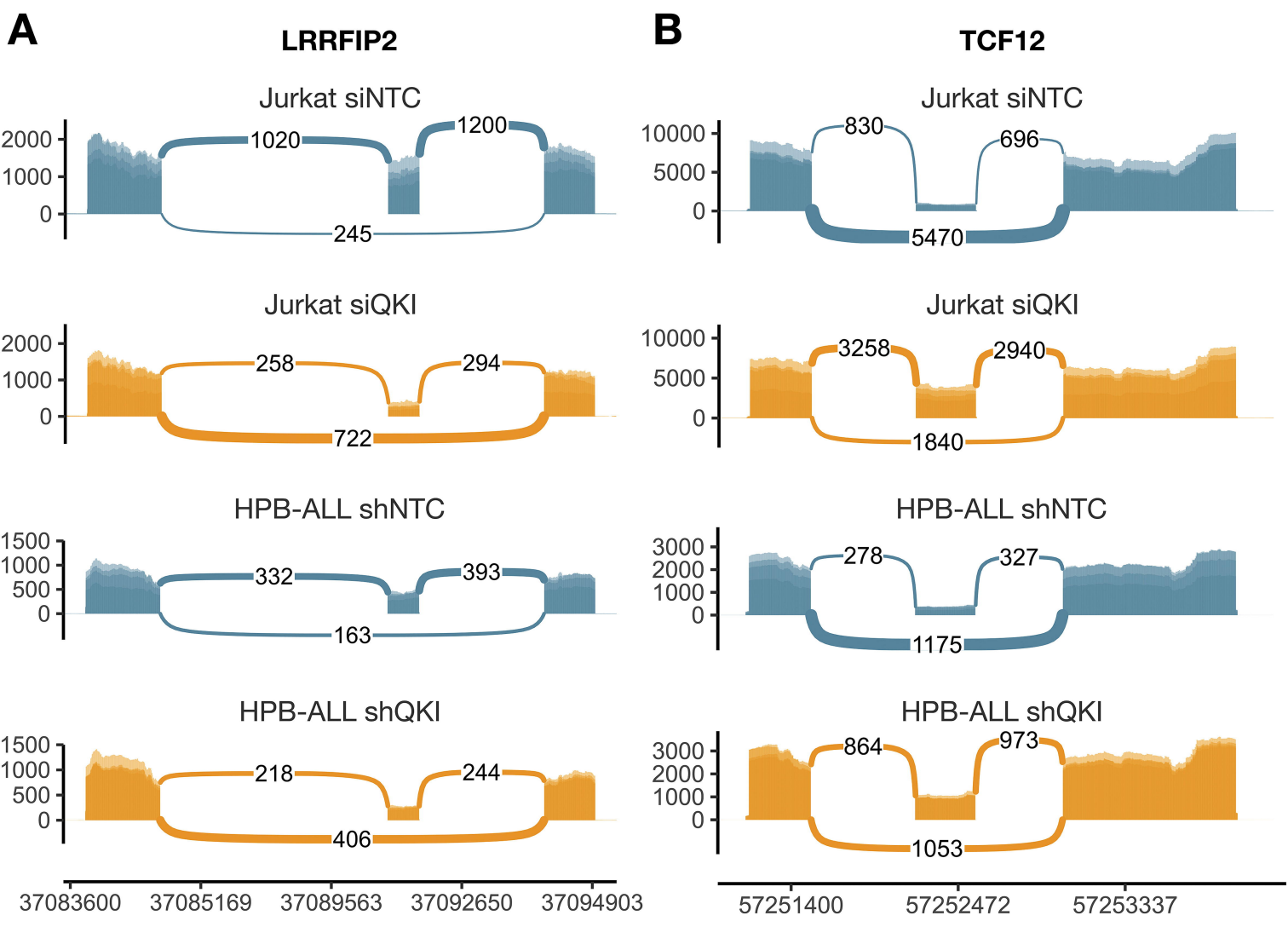
A
LRRFIP2
Jurkat siNTC
2000
1000
0
1020
1200
245
Jurkat siQKI
2000
1000
0
258
294
722
HPB-ALL shNTC
1500
1000
500
0
332
393
163
HPB-ALL shQKI
1500
1000
500
0
218
244
406
37083600
37085169
37089563
37092650
37094903
B
TCF12
Jurkat siNTC
10000
5000
0
830
696
5470
Jurkat siQKI
10000
5000
0
3258
2940
1840
HPB-ALL shNTC
3000
2000
1000
0
278
327
1175
HPB-ALL shQKI
3000
2000
1000
0
864
973
1053
57251400
57252472
57253337

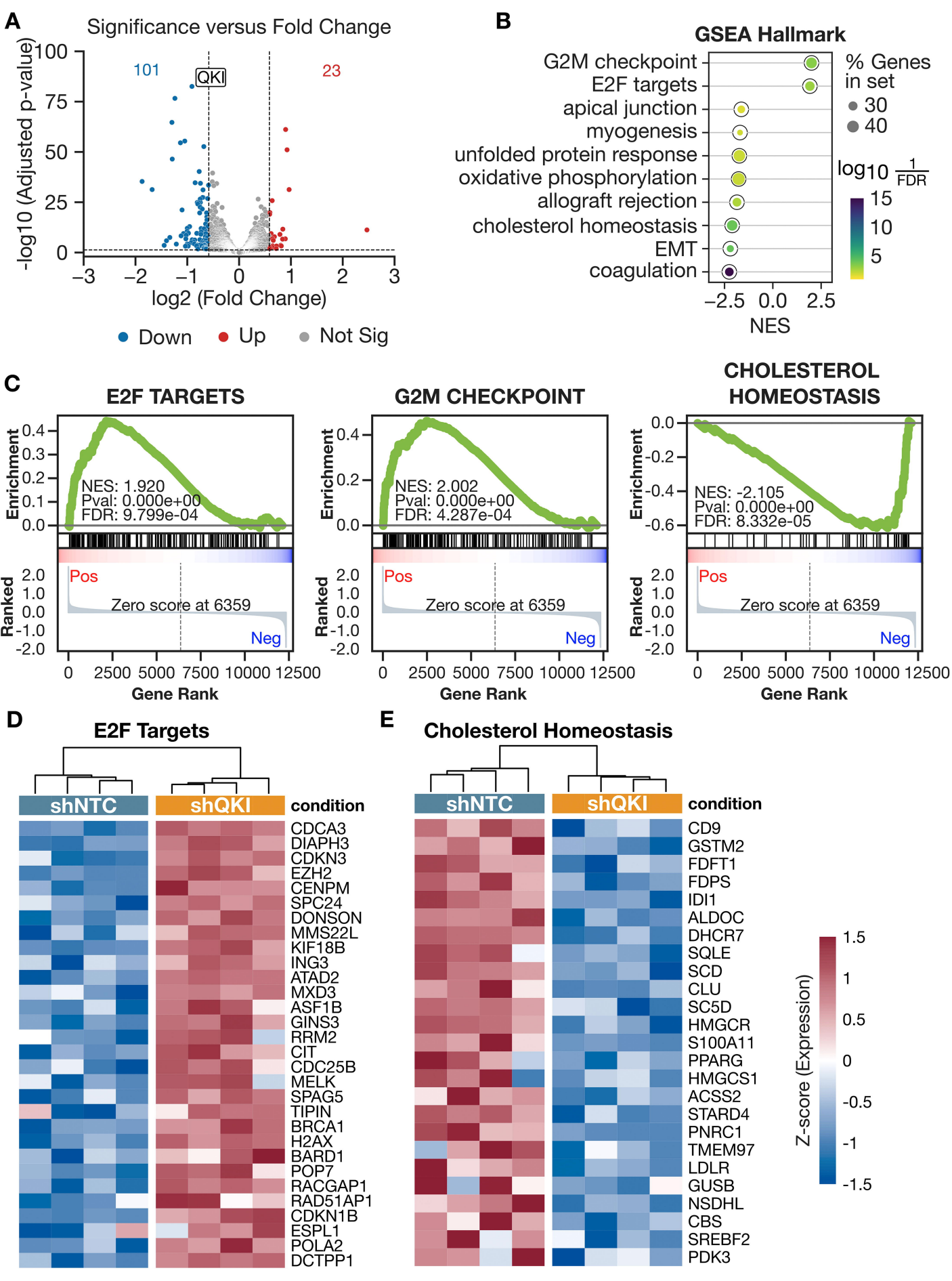
A
Significance versus Fold Change
-log10 (Adjusted p-value)
log2 (Fold Change)
101
23
QKI
Down
Up
Not Sig
B
GSEA Hallmark
G2M checkpoint
E2F targets
apical junction
myogenesis
unfolded protein response
oxidative phosphorylation
allograft rejection
cholesterol homeostasis
EMT
coagulation
% Genes in set
30
40
log10 1/FDR
NES
C
E2F TARGETS
G2M CHECKPOINT
CHOLESTEROL HOMEOSTASIS
Enrichment
NES: 1.920
Pval: 0.000e+00
FDR: 9.799e-04
NES: 2.002
Pval: 0.000e+00
FDR: 4.287e-04
NES: -2.105
Pval: 0.000e+00
FDR: 8.332e-05
Ranked
Pos
Neg
Zero score at 6359
Gene Rank
D
E2F Targets
E
Cholesterol Homeostasis
shNTC
shQKI
condition
CDCA3
DIAPH3
CDKN3
EZH2
CENPM
SPC24
DONSON
MMS22L
KIF18B
ING3
ATAD2
MXD3
ASF1B
GINS3
RRM2
CIT
CDC25B
MELK
SPAG5
TIPIN
BRCA1
H2AX
BARD1
POP7
RACGAP1
RAD51AP1
CDKN1B
ESPL1
POLA2
DCTPP1
CD9
GSTM2
FDFT1
FDPS
IDI1
ALDOC
DHCR7
SQLE
SCD
CLU
SC5D
HMGCR
S100A11
PPARG
HMGCS1
ACSS2
STARD4
PNRC1
TMEM97
LDLR
GUSB
NSDHL
CBS
SREBF2
PDK3
Z-score (Expression)

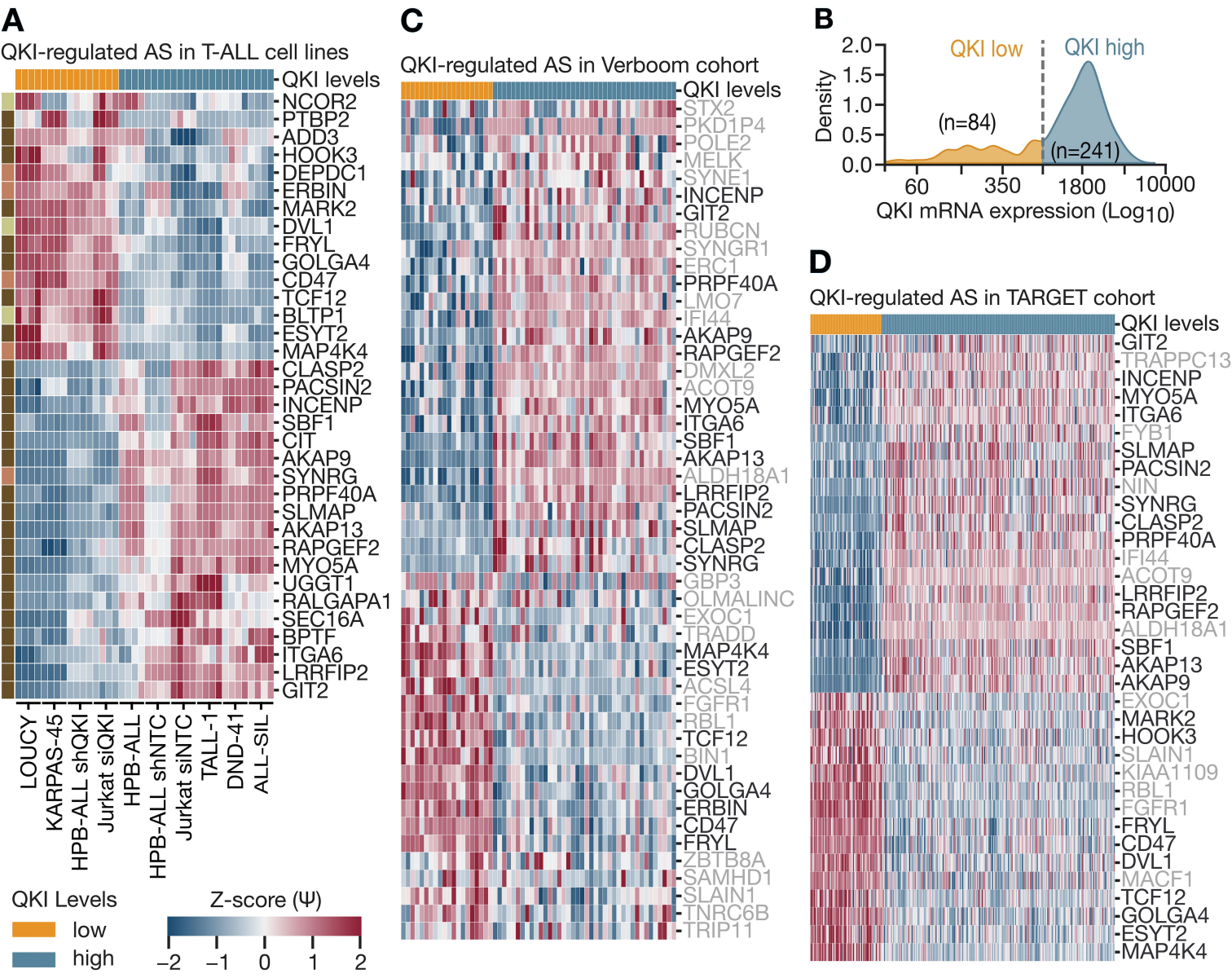
A
QKI-regulated AS in T-ALL cell lines
QKI levels
NCOR2
PTBP2
ADD3
HOOK3
DEPDC1
ERBIN
MARK2
DVL1
FRYL
GOLGA4
CD47
TCF12
BLTP1
ESYT2
MAP4K4
CLASP2
PACSIN2
INCENP
SBF1
CIT
AKAP9
SYNRG
PRPF40A
SLMAP
AKAP13
RAPGEF2
MYO5A
UGGT1
RALGAPA1
SEC16A
BPTF
ITGA6
LRRFIP2
GIT2
LOUCY
KARPAS-45
HPB-ALL shQKI
Jurkat siQKI
HPB-ALL
HPB-ALL shNTC
Jurkat siNTC
TALL-1
DND-41
ALL-SIL
QKI Levels
low
high
Z-score (Ψ)
−2
−1
0
1
2
C
QKI-regulated AS in Verboom cohort
QKI levels
STX2
PKD1P4
POLE2
MELK
SYNE1
INCENP
GIT2
RUBCN
SYNGR1
ERC1
PRPF40A
LMO7
IFI44
AKAP9
RAPGEF2
DMXL2
ACOT9
MYO5A
ITGA6
SBF1
AKAP13
ALDH18A1
LRRFIP2
PACSIN2
SLMAP
CLASP2
SYNRG
GBP3
OLMALINC
EXOC1
TRADD
MAP4K4
ESYT2
ACSL4
FGFR1
RBL1
TCF12
BIN1
DVL1
GOLGA4
ERBIN
CD47
FRYL
ZBTB8A
SAMHD1
SLAIN1
TNRC6B
TRIP11
B
QKI low
QKI high
Density
2.0
1.5
1.0
0.5
0.0
(n=84)
(n=241)
60
350
1800
10000
QKI mRNA expression (Log10)
D
QKI-regulated AS in TARGET cohort
QKI levels
GIT2
TRAPPC13
INCENP
MYO5A
ITGA6
FYB1
SLMAP
PACSIN2
NIN
SYNRG
CLASP2
PRPF40A
IFI44
ACOT9
LRRFIP2
RAPGEF2
ALDH18A1
SBF1
AKAP13
AKAP9
EXOC1
MARK2
HOOK3
SLAIN1
KIAA1109
RBL1
FGFR1
FRYL
CD47
DVL1
MACF1
TCF12
GOLGA4
ESYT2
MAP4K4

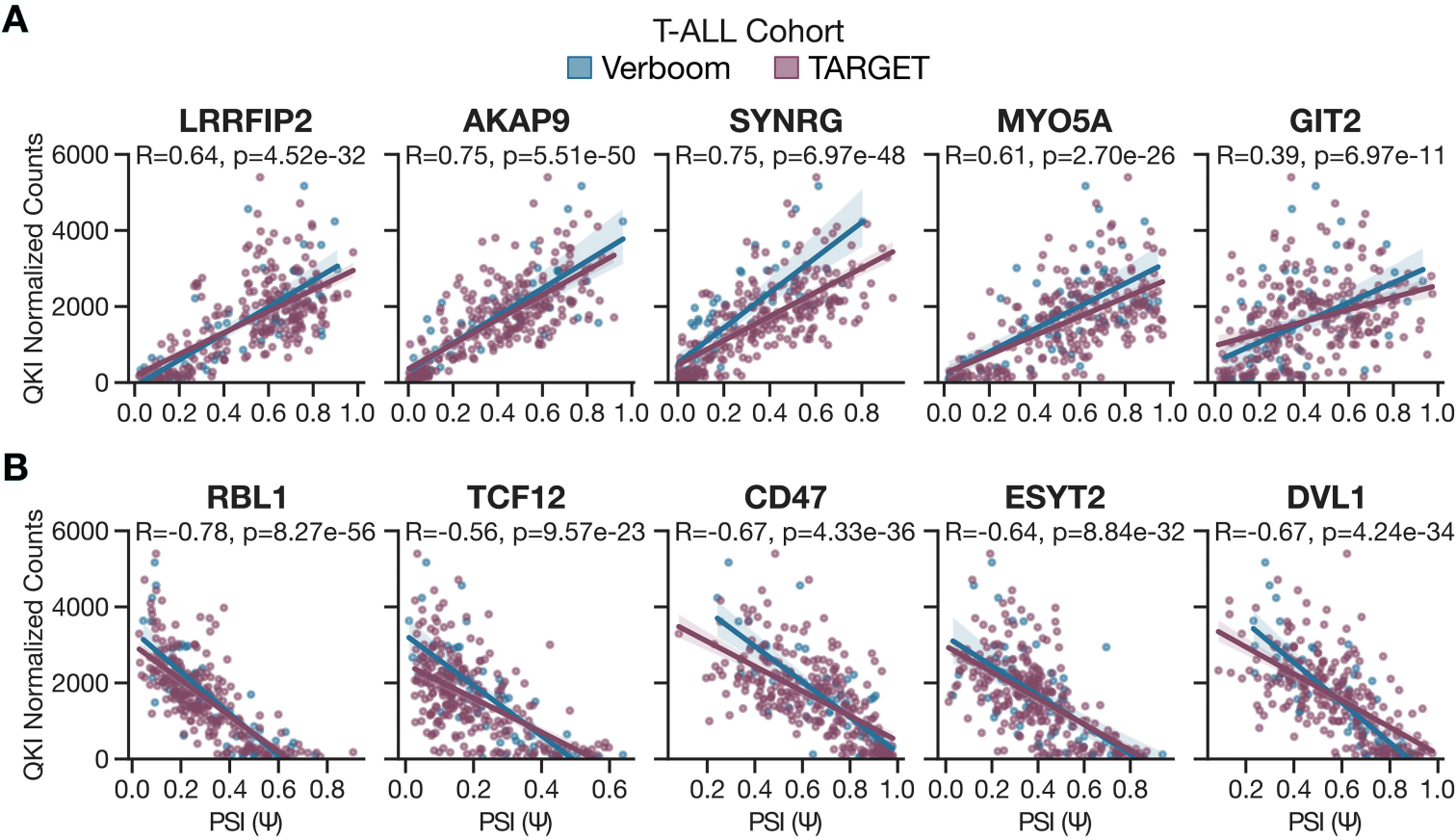
A
T-ALL Cohort
Verboom
TARGET
LRRFIP2
R=0.64, p=4.52e-32
AKAP9
R=0.75, p=5.51e-50
SYNRG
R=0.75, p=6.97e-48
MYO5A
R=0.61, p=2.70e-26
GIT2
R=0.39, p=6.97e-11
QKI Normalized Counts
6000
4000
2000
0
0.0 0.2 0.4 0.6 0.8 1.0
B
RBL1
R=-0.78, p=8.27e-56
TCF12
R=-0.56, p=9.57e-23
CD47
R=-0.67, p=4.33e-36
ESYT2
R=-0.64, p=8.84e-32
DVL1
R=-0.67, p=4.24e-34
PSI (Ψ)

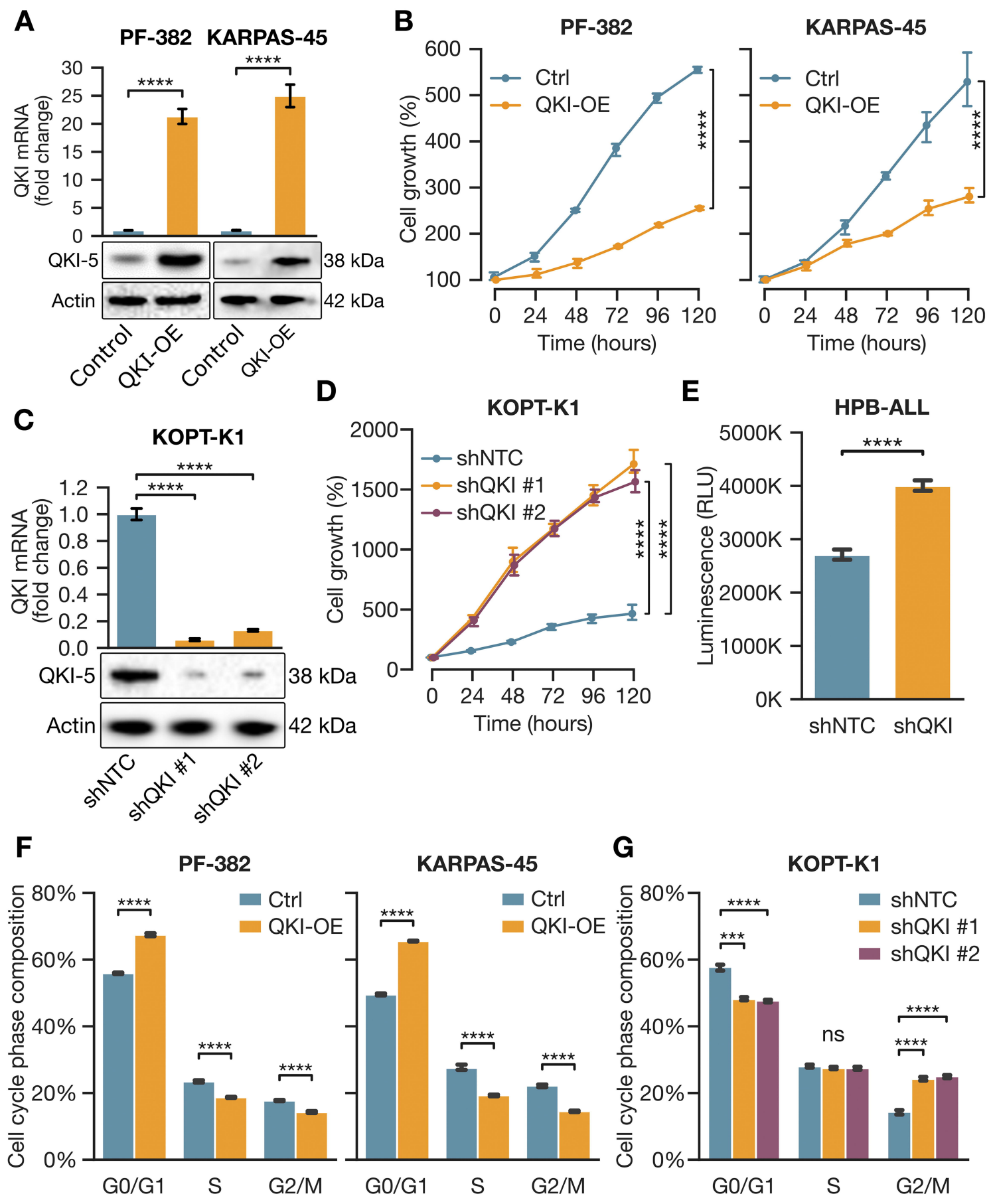
A
PF-382
KARPAS-45
QKI mRNA (fold change)
****
QKI-5
Actin
38 kDa
42 kDa
Control
QKI-OE
B
PF-382
KARPAS-45
Cell growth (%)
Ctrl
QKI-OE
Time (hours)
C
KOPT-K1
shNTC
shQKI #1
shQKI #2
D
E
HPB-ALL
Luminescence (RLU)
F
G
Cell cycle phase composition
G0/G1
S
G2/M
ns
***

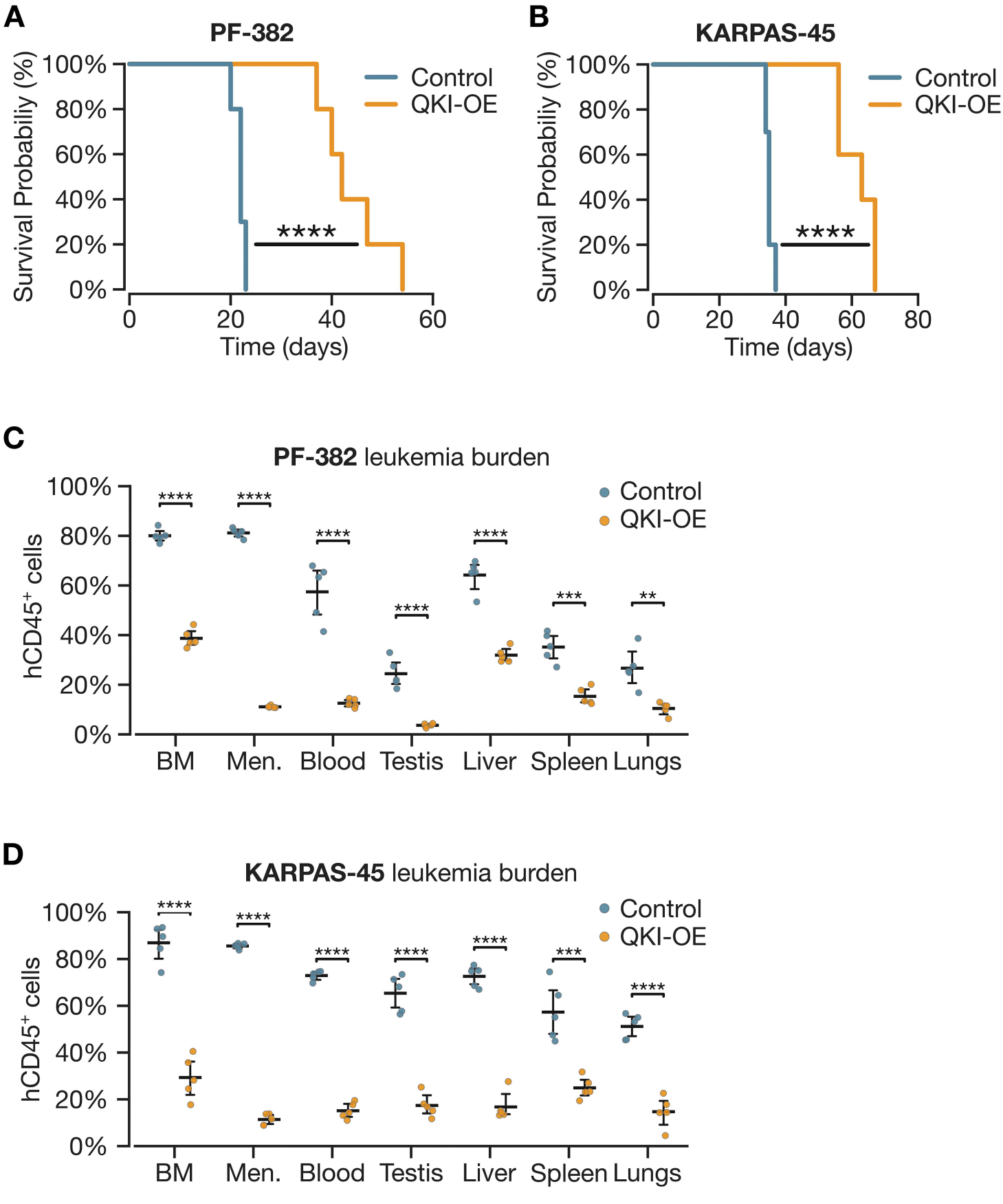
A
PF-382
Survival Probability (%)
100%
80%
60%
40%
20%
0%
0
20
40
60
Time (days)
Control
QKI-OE
****
B
KARPAS-45
Survival Probability (%)
100%
80%
60%
40%
20%
0%
0
20
40
60
80
Time (days)
Control
QKI-OE
****
C
PF-382 leukemia burden
hCD45+ cells
100%
80%
60%
40%
20%
0%
Control
QKI-OE
****
****
****
****
****
***
**
BM
Men.
Blood
Testis
Liver
Spleen
Lungs
D
KARPAS-45 leukemia burden
hCD45+ cells
100%
80%
60%
40%
20%
0%
Control
QKI-OE
****
****
****
****
****
***
****
BM
Men.
Blood
Testis
Liver
Spleen
Lungs

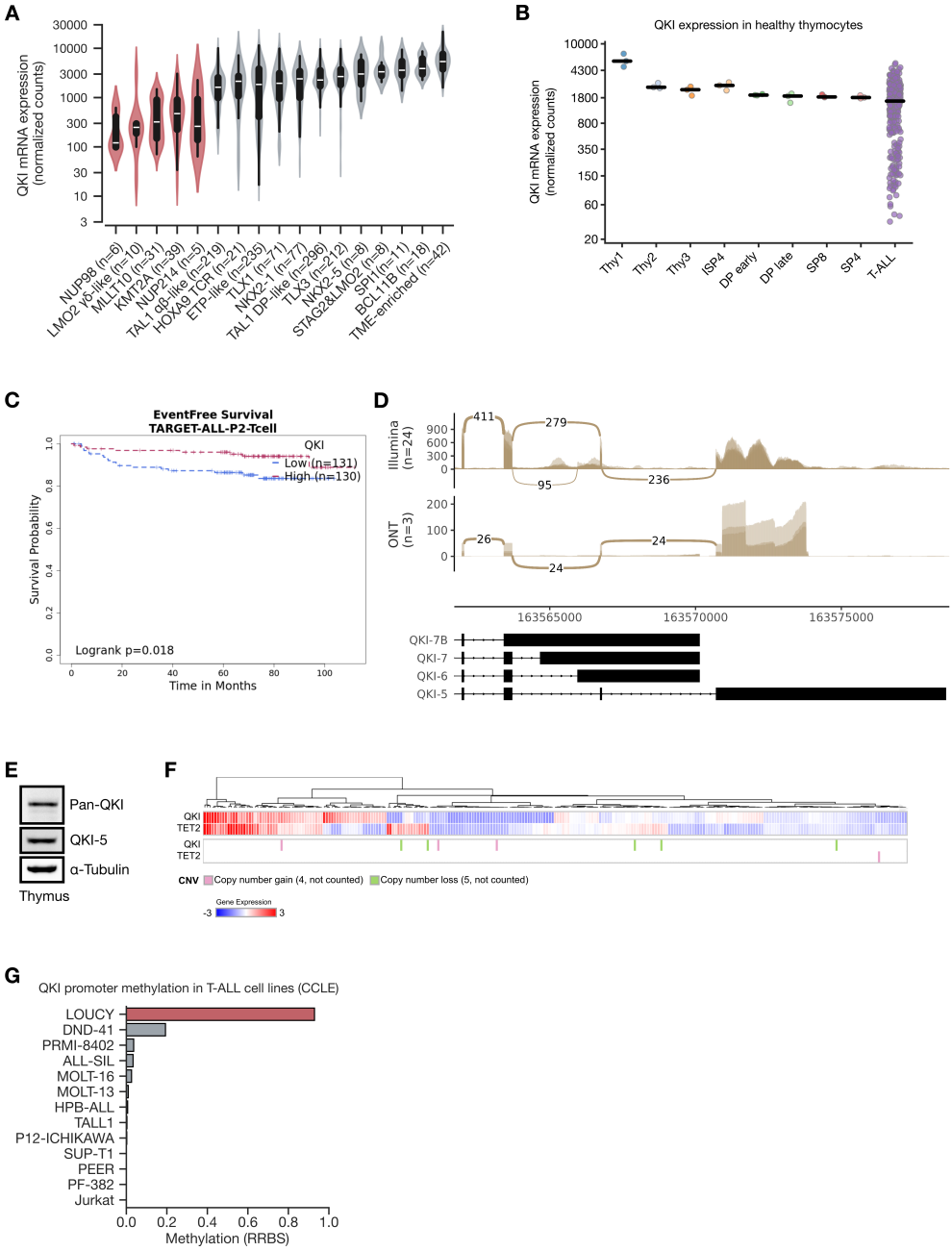

Supplementary Figure. 1: Analysis of *QKI* expression and genetic alterations in T-ALL and healthy thymocytes. (A) *QKI* mRNA expression across molecular subtypes from the Pölönen et al. (Nature 2024) cohort, showing subtype-specific variation. (B) *QKI* expression levels across different stages of thymocyte development (Thy1, Thy2, Thy3, ISP4, DP early, DP late, SP8, SP4), showing that *QKI* levels remains relatively constant in healthy thymocytes compared to T-ALL patient samples. (C) Kaplan-Meier plot displaying event free survival of T-ALL patients (TARGET) stratified into QKI-low and QKI-high. (D) Sashimi plots representing the splicing pattern of *QKI* using short-read sequencing (Illumina) from 24 healthy thymi samples and long-read sequencing (ONT) from 3 healthy thymi samples. The unique C-terminal end of each *QKI* isoform is shown below. Both sequencing technologies support the expression of QKI-5 as the main isoform, with QKI-6 detected to a much lesser extent only with short-read sequencing. (E) Western blot of QKI isoforms in a healthy thymus sample, using QKI-5, Pan-QKI and α-Tubulin as loading controls. (F) A heatmap illustrating *QKI* and *TET2* gene expression in T-ALL patient samples, highlighting similar expression patterns between the two genes across various patients. Below is copy number variation (CNV) and mutational burden analysis, showing instances of copy number gains and losses for *QKI* and *TET2* in T-ALL samples. (G) Bar plot depicting the levels of QKI promoter methylation, measured by reduced representation bisulfite sequencing (RRBS), across various T-ALL cell lines from the Cancer Cell Line Encyclopedia (CCLE).

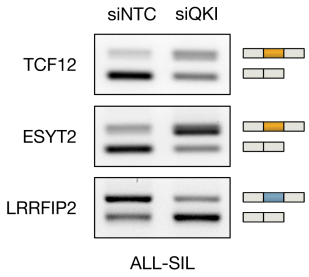

Supplementary Figure. 2: RT-PCR validation of QKI-dependent splicing events in ALL-SIL cells transfected with siNTC (control) or siQKI. Exon inclusion was assessed for *TCF12*, *ESYT2*, and *LRRFIP2* transcripts. The results confirm that QKI knockdown leads to altered splicing patterns in these genes, consistent with RNA-seq data.

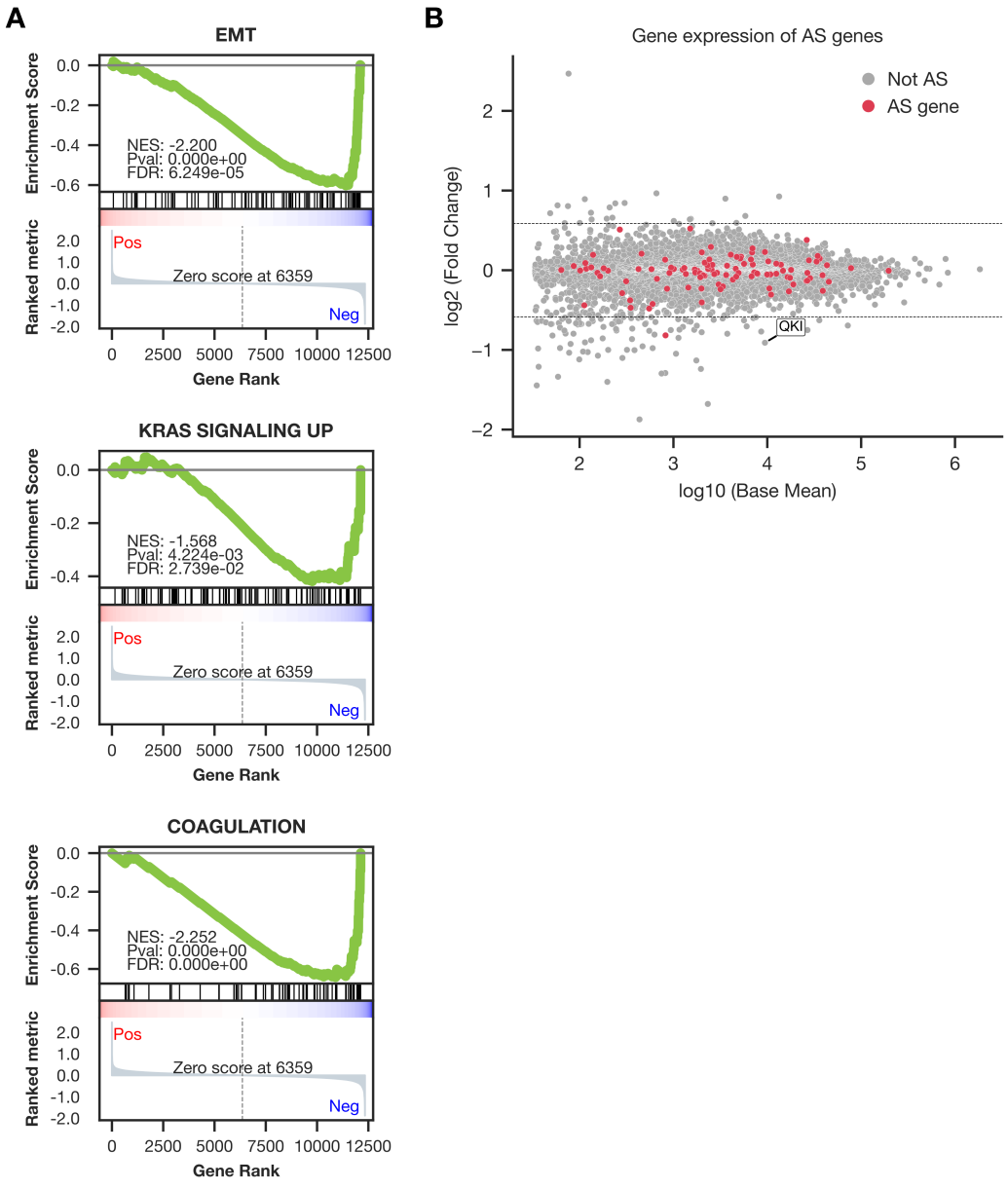

Supplementary Figure. 3: Gene set enrichment analysis (GSEA) and differential expression analysis following QKI silencing in HPB-ALL cells. (A) GSEA plots showing significant negative enrichment of hallmark gene sets for epithelial-mesenchymal transition (EMT), KRAS signaling up, and coagulation in QKI-depleted HPB-ALL cells. The normalized enrichment scores (NES), false discovery rates (FDR), and p-values indicate the significance of these pathway changes upon QKI silencing. (B) MA plot displaying the differential expression of genes following QKI knockdown. The plot highlights $\log_2$ fold changes relative to the mean expression across all genes. Alternatively spliced (AS) genes is marked in red, showcasing the relationship between differential splicing and expression changes.

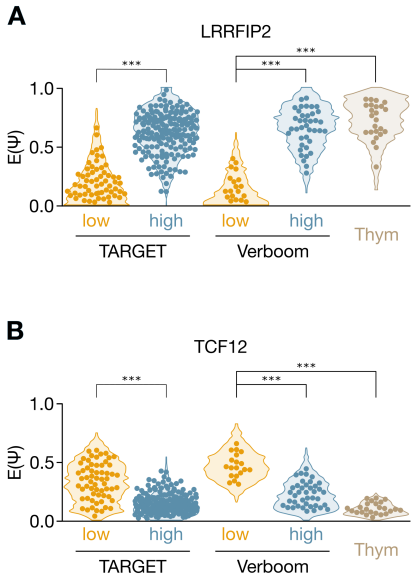

Supplementary Figure. 4: QKI-regulated splicing in *LRRFIP2* and *TCF12* across T-ALL cohorts and thymocytes. (A) Violin plots representing the expected percent spliced-in (E[Ψ]) values for the *LRRFIP2* alternative splicing event in the TARGET cohort (low vs. high expression groups) and the Verboom dataset (low vs. high expression groups), alongside thymocyte (Thym) samples as a reference. (B) Violin plots showing the E[Ψ] values for the *TCF12* alternative splicing event across the same cohorts and conditions. Statistical significance between groups was determined using the Mann-Whitney U test (***: $p < 0.001$).

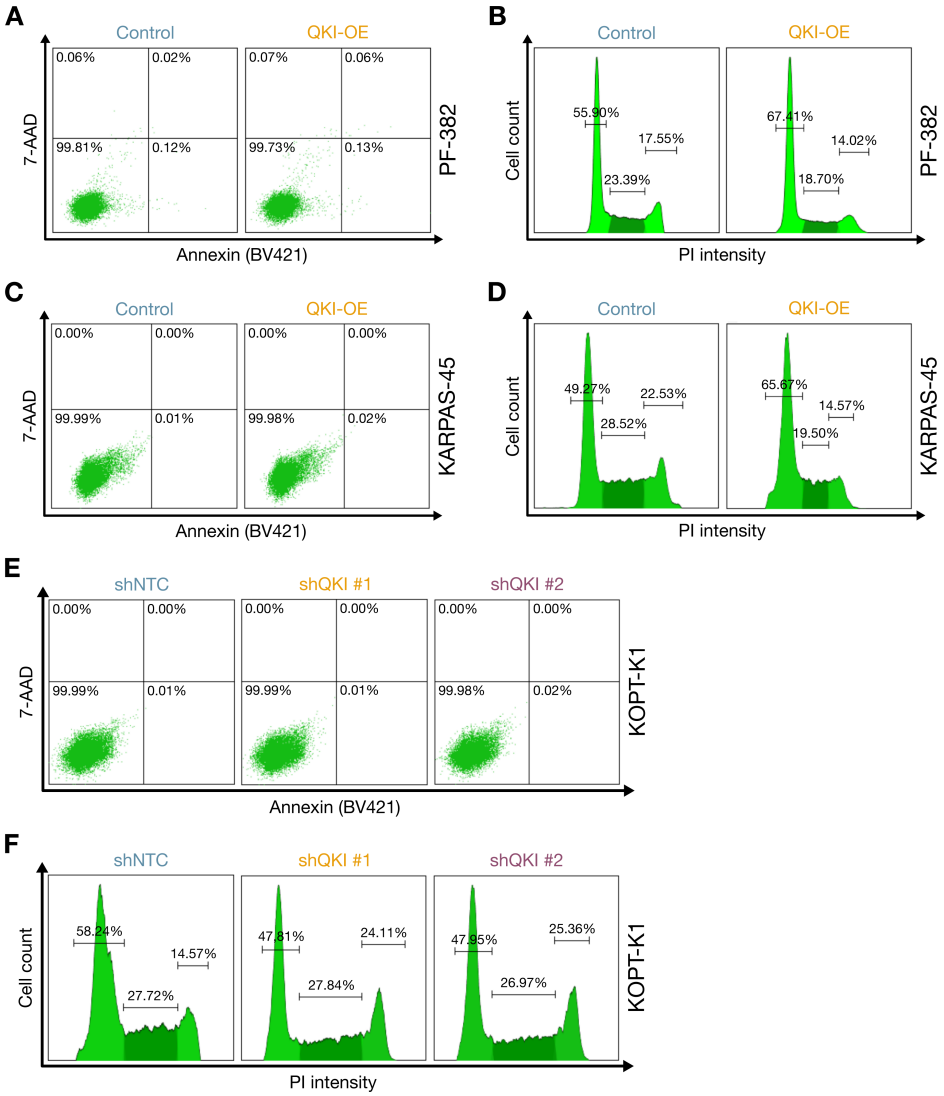

Supplementary Figure. 5: Apoptosis and cell-cycle analysis in QKI-overexpressing and QKI-depleted T-ALL cell lines. (A) Flow cytometry analysis of apoptosis in control and QKI-overexpressing (QKI-OE) PF-382 cells using Annexin V/7-AAD staining. The percentage of cells in early and late apoptosis is shown. No significant difference in apoptosis levels was observed between the two groups. (B) Cell cycle analysis of control and QKI-OE PF-382 cells by propidium iodide (PI) staining, showing an increased proportion of QKI-OE cells in the G0/G1 phase. (C) Annexin V/7-AAD staining of control and QKI-OE KARPAS-45 cells, showing no significant changes in apoptosis. (D) PI-based cell cycle analysis of KARPAS-45 cells, demonstrating a higher G0/G1 fraction in QKI-OE cells compared with controls. (E) Annexin V/7-AAD staining of KOPT-K1 cells transduced with non-targeting shRNA (shNTC) or QKI-targeting shRNAs (shQKI #1, shQKI #2), showing no increase in apoptosis upon QKI depletion. (F) PI-based cell cycle profiles of KOPT-K1 cells, showing reduced G0/G1 fractions in QKI-depleted cells compared with shNTC controls.

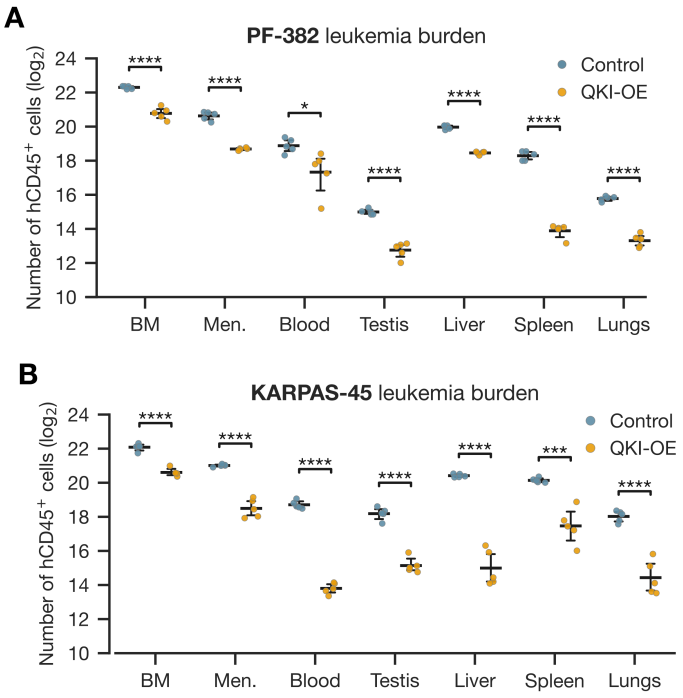

Supplementary Figure. 6: QKI overexpression prolongs survival in T-ALL xenografts. (A) Leukemia burden in NSG mice engrafted with PF-382 T-ALL cells (10^6 cell/mouse via tail vein) expressing either a control vector or QKI (QKI-OE) , quantified at Day 23 post-engraftment by the number of of human $CD45^+$ cells infiltrating bone marrow (BM), meninges (Men.), blood, testis, liver, spleen and lungs. (B) Leukemia burden in NSG mice engrafted with KARPAS-45 T-ALL cells expressing either control or QKI-OE, measured as in panel A. Statistical significance was determined using unpaired Student's t-test with Holm-Sidak multiple comparison correction (**: $p < 0.01$; ***: $p < 0.001$; ****: $p < 0.0001$).

Supplementary Material and Methods

QKI silencing in Jurkat and KOPT-K1 cells

Transfection was performed using the Neon transfection system (Thermo Fisher) and the device was set to 1325V, 10 ms, 3 pulses. Approximately $4x10^6$ cells were transfected with 20 nM of either an NTC or QKI siRNA (ON-TARGETplus SMARTpool siRNA; Dharmacon®). 72 hours post-transfection, total RNA was extracted and isolated using the RNeasy Plus mini kit (QIAGEN) according to manufacturer's instructions. The experiment was repeated 4 times. The two pre-designed shRNA targeting QKI (TR302174V) and a scrambled control (shNTC) (TR30021V) were purchased from Origene (Rockville, MD, USA). The sequences are: shQKI # 1: TTCAGTTACAAGAGAAACTTTATGTGCCT and shQKI # 2: ACTAATCACTGTGGAAGATGCTCAGAACA. The packaging vectors and recombinant expression plasmids were co-transfected into 293FT cells using Lipofectamine 2000 (Thermo Fisher Scientific). After 48 hours, viral supernatants were collected and titrated. Lentiviral particles were then mixed with 8 µg/ml Polybrene and applied to T-ALL cell lines at a multiplicity of infection (MOI) of 10. Following centrifugation, cells were selected with puromycin for approximately three weeks. GFP expression was analyzed on a FACSAria flow cytometer, and cells were sorted if the infection efficiency was below 85%.

QKI overexpression in KARPAS-45 and PF-382 cells

The recombinant expression plasmid Precision LentiORF QKI (QKI-OE) (OHS5900-202626095) and the corresponding control vector (OHS5833) were obtained from Dharmacon (Lafayette, CO, USA). Lentiviral packaging vectors pMD2.G, pMDLg/pRRE, and pRSV-Rev were purchased from Addgene (Cambridge, MA, USA). The transduction was performed as described above.

QKI knockdown in HPB-ALL

HEK293 cells were cotransfected with the envelope (pMD2.G), packaging (psPAX2) and the shRNA TRC vector (MISSION®) harboring either a non-targeting shRNA or an shRNA targeting QKI (TRCN0000233373). Viral particles were collected 72h and 96h post-transfection and concentrated 10 times using PEG-it (system biosciences). HPB-ALL cells were transduced with these viral particles by spinoculation (2300 rpm, 90 min, 32°C) in the presence of 8 µg/mL polybrene (Sigma, H9268). After 72 hours, 1 µg/mL of puromycin was included in the culturing media for the selection of transduced cells, for 7 days. Total RNA was extracted as above. The experiment was performed 4 times.

RT-qPCR

Reverse transcription was performed using iScript™ cDNA Synthesis Kit (BioRad) with 1 µg of RNA and input. qPCR was performed with the SsoAdvanced Universal SYBR® Green Supermix (BioRad, 1725275) under standard PCR conditions on a LightCycler® 480 System (Roche). The data was normalized and analyzed in the QBase+ software (CellCarta).

Cell viability assay

Cell viability was assessed using the CellTiter 96 AQueous One Solution Cell Proliferation Assay (MTS) (Promega, Madison, WI, USA). Using an Agilent BioTek 800 TS Microplate Absorbance Reader, the absorbance was measured at 490 nm.

Apoptosis and cell cycle

In 6-well plates, 10^6 T-ALL cells were cultured for 48 hours. Cells were washed in binding buffer and stained with 5 µl of Annexin V conjugated to BV421 and 5 µl of 7-ADD (BD Pharmingen, San Jose, CA, USA) for 15 minutes at RT in the dark. For cell cycle study, cells were frozen and permeable in 70% ethanol for 2 hours at -20°C. They were then treated with propidium iodide/RNase Staining Buffer (BD Pharmingen) for 15 minutes at RT. The stained cells were evaluated using flow cytometry and quantified using FlowJo software.